Speed Control of Switched Reluctance Motors

A thesis submitted to
The Hong Kong University of Science and Technology
in partial fulfillment of the requirements for
the Degree of Master of Philosophy in
Electrical and Electronic Engineering

By

GAO Yuan

Department of Electrical and Electronic Engineering
The Hong Kong University of Science and Technology

Aug, 2000

Speed Control of Switched Reluctance Motors

by

GAO Yuan

Approved by:

Dr. Li QIU
Thesis Supervisor

Dr. Zexiang LI
Thesis Examination Committe Member (Chairman)

Dr. Li-Xin WANG
Thesis Examination Committe Member

Prof. Philip C.H. Chan
Head of Department

Department of Electrical and Electronic Engineering
The Hong Kong University of Science and Technology

Aug 2000

Speed Control of Switched Reluctance Motors

by

GAO Yuan

for the Degree of
Master of Philosophy in Electrical and Electronic Engineering
at The Hong Kong University of Science and Technology
in Aug, 2000

Abstract

Nowadays, switched reluctance motors (SRMs) attract more and more attention. The switched reluctance motor is simple to construct. It not only features a salient pole stator with concentrated coils, which allows earlier winding and shorter endturns than other types of motors, but also features a salient pole rotor, which has no conductors or magnets and is thus the simplest of all electric machine rotors. Simplicity makes the SRM inexpensive and reliable, and together with its high speed capacity and high torque to inertia ratio, makes it a superior choice in different applications.

However, the control of the SRM is not an easy task. The motor's double salient structure makes its magnetic characteristics highly nonlinear. The motor flux linkage appears to be a nonlinear function of stator currents as well as rotor position, as does the generated electric torque. Apart from the complexity of the model, the SRM should be operated in a continuous phase-to-phase switching mode for proper motor control. The torque ripple and noise as a result of this commutation are the other two awkward issues which have to be tackled. All these make the control of the SRM a tough challenging.

This thesis attempts to investigate the control of the switched reluctance motor from the motor's structure properties, model equations, operation prin-

ciple, power converter topology and commutation algorithms to starting problem.

Apart from the general introduction, this thesis focuses on speed control of an 8/6 SRM based on a simplified model. This simplified model limits the operation of the motor completely into its linear flux region. According to this model, two different commutation strategies, two-phase-exciting and single-phase-exciting methods, are discussed in details. It has been observed that, not like the two-phase-exciting, the turn-on angle for single-phase-exciting is not trivial for it will affect the system performance. Consequently, an optimized single-phase-exciting method is proposed. This method optimizes the whole system's performance from the point of view of power efficiency of the whole system. By optimizing the average power of the whole system, the motor's transient as well as steady-state performance for speed tracking can be improved simultaneously.

Experimental results supported the proposed method. These results compared the influences of the two-phase-exciting strategy, optimized and non-optimized single-phase-exciting method on speed tracking capacity and stator currents. It showed that the optimized single-phase has almost the same speed tracking capacity as two-phase-exciting strategy, and the peak value of their stator currents is at the same level under the same condition. However, the performance in speed tracking by the non-optimized single-phase-exciting method is much worse than the other two under the same condition. The reason for this phenomenon has been analysed.

Acknowledgments

I would like to express my sincere thanks to Dr. Li QIU, my supervisor. His motivation and encouragement kept me going throughout this thesis. His patience and support have been invaluable towards the completion of this work. I would also like to thank my committee members, Dr. Zexiang LI and Dr. Li-xin WANG for their guidance and comments on my thesis.

I am indebted to all my esteemed colleagues for helping me in various ways. I am most grateful to Mr. Wai-Chuen GAN for discussing and sharing his ideas with me. I would like to take the opportunity to thank Mr. Y.K. Yiu for his technical support. My gratitude also goes to many other people such as Ms. Yang Rong, Ms. Chen Hui, Ms. Li Tao, Mr. Jiang Shillong, Mr. Liu Guanfeng and Mr. Xiong Zhenghua for their sincere friendship and encouragement.

Moreover, I dedicate this thesis to my parents, my little sister and brother for their support and blessing in every aspect of my life.

Contents

List of Figures

Chapter 1

Introduction

1.1 Overview

At an age of more than 150 years, and counting, the switched reluctance motor (SRM) represents one of the oldest electric motor designs around.

Partly as a result of recent demand for variable-speed drives and primarily as a result of the development of power semiconductors, a variation on the conventional reluctance machine has been developed and is know as the "switched reluctance" (SR) machine. The name "switched reluctance", first used by one of the authors of [1], describes the two features of the machine configuration: (a). switched — the machine must be operated in a continuous switching mode, which is the main reason the machine developed only after good power semiconductors became available; (b). reluctance — it is the true reluctance machine in the sense that both rotor and stator have variable reluctance magnetic circuits, or, more properly, it is a double salient machine.

The concept of the switched reluctance machine is actually very old, going back to the 19th century inventions called "electromagnetic engines" [2], which were the forerunners of modern stepper motors. The switched reluctance motor is basically a stepper motor and has had many applications as both rotary and linear steppers. The idea of using the SR configuration in a continuous mode (on contrast to a stepper mode) with power semiconductor

control is due primarily to Nasar [1], French [3], Koch [4] and Lawrenson [5] in the 1960's. At that time, only thyristor power semiconductors were available for the relatively high-current, high-voltage type of control needed for SR machines. These years, power transistors, GTOs, IGBTs, and power MOSFETs have been developed in the power ranges required for SRM control.

Simple construction is a prime feature. SR motors eliminate permanent magnets (PMs), brushes and commutators. The stator consists of steel laminations forming salient poles. A series of coil windings, independently connected in phase pairs, envelops the stator poles. With no rotor winding, the rotor is basically a piece of steel (and laminations) shaped to form salient poles. It is the only motor type with salient poles in both the rotor and stator (double salient). As a result, and also because of its inherent simplicity, the SR machine promises a reliable and low-cost variable-speed drive and will undoubtedly take the place of many drives now using the cage induction and DC commutator machines in the short future.

1.2 Advantages and Applications of Switched Reluctance Motors

SR motors offer numerous benefits, such as:

♦ Performance — much greater torque output and with the same (or slightly higher) efficiencies than "premium efficiency" induction motors. Efficiency is flat over a wider speed range;

♦ Small unit size — makes efficient use of materials and low inertia;

♦ Low cost — low manufacturing cost, low material cost and low maintains cost. It does not use magnets;

♦ High speed and acceleration capability — 100,000RPM (Rotation Per Minute), with the proper drive;

♦ Cooling — most of the heat is generated in stationary stator which is relatively easy to cool;

♦ Rugged construction suitable for harsh environments such as high temperature and vibration.

SRM controllers add to the benefits. Since they do not need bipolar (reversed) currents, the number of power-switching devices can be reduced by 50%, compared to bridge-type inverters of adjustable-speed drives. An SRM drive has inherent reliability and fault tolerance, it can run in a "limp-home" mode with diminished performance with one failed transistor in a phase, unlike standard motor drives.

As control techniques developed, applications of SRMs include:

(a). general purpose industrial drives;

(b). application-specific drives: compressors, fans, pumps, centrifuges;

(c). domestic drives: food processors, washing machines, vacuum cleaners;

(d). electric vehicle application;

(e). aircraft applications;

(f). servo-drives.

1.3 Motivation

A good machine drive has to meet the general requirements of four-quadrant operation (i.e., forward/reverse and positive or negative torque), with seamless transition between quadrants. True "servo quality" control imposes further requirements of very low torque ripple, rapid dynamic response, good stability, ability to operate at zero speed, and smooth reversing. Even without these servo-quality requirements, optimized performance for simple variable-speed drives requires continuous control of the firing angles (i.e. the switching on/off angles of power conductors).

The DC commutator motor and the brushless DC motor are well adapted to these advanced requirements because their torque is proportional to current. With vector control (field-oriented control), AC inductance motors and PM synchronous motors effectively acquire this characteristic of the DC mo-

tor. Theoretically, this is possible because the equations of the AC motor can be transformed into those of the DC motor by means of reference-frame transformations (the dq-axis transformation).

The switched reluctance motor has no dq-axis transformation, and no field oriented control principle has been developed for it[1]. Therefore, the requirements of four-quadrant operation and servo performance can only be met by high-speed real-time controllers which operate with phase currents and voltages directly, and not with slow-varying dq-axis quantities. Such high-speed controls are used in advanced DC and AC drives already, in order to achieve the highest dynamic performance. What makes the SRM different is that the relationships between torque, current, speed and firing angles (i.e. the commutation angles) are highly nonlinear and vary as functions of speed and load.

These highly nonlinear relationships of the SRM are due to its single-excited (exciting the stator only) double-salient and highly nonlinear machine characteristics. The generated electrical torque appears to be a high order polynomial of the stator currents with an order equal to or large than two. Even in the simplest case, the electrical torque is not a linear function of the stator current. Moreover, this torque and current relationship of the SRM is usually not as clear as any other types of motors. For this reason, there are many methods modeling this torque-current relationship, such as fuzzy logic, artificial neutral network (ANN) and finite element analysis (FEA) and so on. On the other hand, the generated electrical torque is a function of the rotor position too. In order to achieve desired torque, the motor has to be operated in a phase-to-phase switching mode based on accurate rotor position information. This commutation increases the complexity of the control algorithm. Besides, torque ripple and acoustic noise problems arise with the commutation.

Therefore, this thesis attempts to find solutions to these problems. It

[1]There are some researchers investigating this method. However, it needs very strict assumption and the method is not a universal one. Please refer to [6]-[8] for details.

starts from the simplest case, which is in the linear region of the motor's magnetic characteristics chart. Based on this simplified model, different control algorithms will be investigated. Experimental results will be demonstrated too.

1.4 Contribution of the Thesis

The contribution of this thesis focuses mainly on the following two aspects:

First, this thesis formulated the optimization problem of single-phase-exciting commutation strategy. It is the first time to point out that the exciting moment for single-phase-exciting is not trivial because it significantly affects the final performance of the motor. This thesis proposed an optimized conducting method for the single-phase-exciting commutation strategy by optimizing the average power of the whole system. Meanwhile, the motor's performance can be improved in practical operations by the proposed scheme. Experimental results were given to verify this point.

Besides, in this project, an SRM testing bed has been built up. This testing bed consists of the interface circuits between the host controller and outer driving devices, the current tracking driver and sensoring device. Using this testing bed, one can test different control algorithms for the SRM conveniently without building hardware or designing circuit.

1.5 Outline of the Thesis

This thesis is organized as follows:

Chapter 1 gives a general introduction of switched reluctance motors: its history, advantages and applications. The inherent control problems rising with the motor's special double-salient structure are briefly discussed. Then the motivation of this thesis is given.

In Chapter 2, the principle of the SRM motor is discussed in details from both a physical and mathematical point of view. Its torque equation and model

equations are deduced in Section 2.1; Section 2.2 explains how to operate a SRM from a physical point of view. The principles for proper operation have been concluded in this section.

Differing from any other type of motors, the SRM has its own special properties. The most special one which makes the control of the motor challenging enough is its nonlinear magnetic characteristics. Chapter 3 focuses on this magnetic characteristics. Section 3.1 discusses the SRM's flux-linkage properties; Section 3.2 gives a method to measure this magnetic chart; And section 3.3 specifies how to make use of this magnetic chart to control the machine.

In Chapter 4, the control of the SRM is discussed in detail. First, Section 4.1 gives a model in linear flux region. Section 4.2 describes different power converter topologies for the SRM; In Section 4.3, two exciting methods, the two-phase-exciting and one-phase-exciting commutation are analyzed and compared; Section 4.4 proposed an optimized scheme based on whole system energy for the one-phase-exciting control algorithm. The closed loop system is described in the Section 4.5. And Section 4.6 gives a solution to the start up problem of the SRM.

Chapter 5 deals with the experimental setup hardwares, such as controllers, power converter, position and current sensoring devices and the SRM used in this thesis.

Experimental results are demonstrated in Chapter 6. Some conclusions are drawn based on these results.

Chapter 7 concludes the whole thesis and proposes further research.

Chapter 8 is the photo album of this project.

Chapter 2

Mathematical Model of SR Motors

The SRM does obey the laws of physics. The torque in a reluctance motor is developed by virtue of the change in the reluctance with respect to the rotor position. Based on this principle, a reluctance motor is different from other types of electric machines such as the DC machine, synchronous machine and induction machine.

The theory of conventional reluctance machines evolved from synchronous machine theory developed in the early 20th century, based on the well-known Park equations. The theory for SRMs developed from a simpler, circuit-theory approach in the second half of 20th century. The basic torque or force production in reluctance machines results from the variation of the stored magnetic energy as a function of the rotor position. This relationship also applies to most electromagnetic relays, holding magnets, solenoid actuators, and other devices where force is produced between two magnetic surfaces, including all machines with saliency.

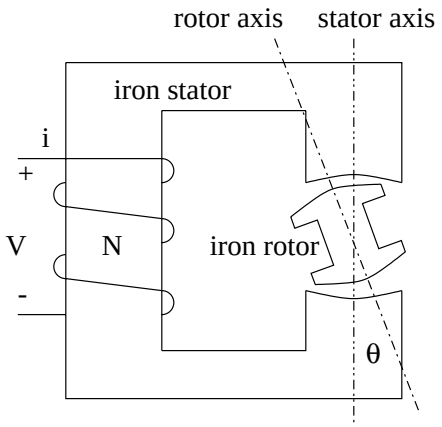

Figure 2.1: A Single Phase SRM

2.1 Mathematics Equations of the SRM

2.1.1 Torque Equation

To derive the basic torque equation of the SRM, let us consider an elementary reluctance machine as shown in Figure 2.1. The machine is single phase exited; that is, it carries only one winding on the stator. The excited winding is wound on the stator and the rotor is free to rotate.

The flux linkage is

$$\lambda(\theta) = L(\theta)i \tag{2.1}$$

where i is the independent input variable, i.e. the current flows through the stator.

The general torque expression is then given by [9]

$$T_e = \left[\frac{\partial W^{'}}{\partial \theta}\right]_{i=const} \tag{2.2}$$

where $W^{'}$ is the *coenergy*. At any position the coenergy is the area below the magnetization curve as shown in Figure 2.2, in other words, the definite integral

$$W^{'} = \int_0^{i_1} \lambda(\theta, i)di \tag{2.3}$$

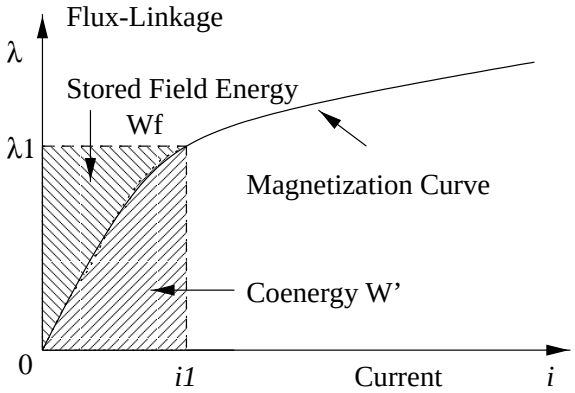

Figure 2.2: Flux-Linkage Chart

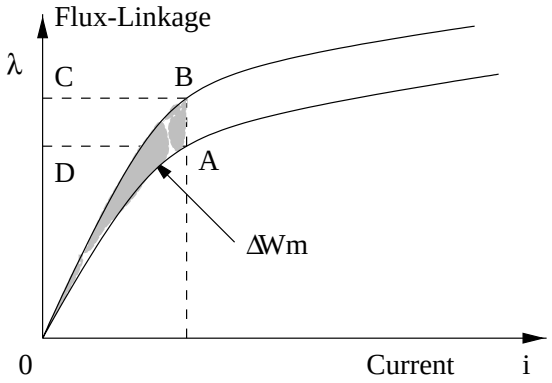

Figure 2.3: Diagram of Energy Exchange

So the torque equation (2.2) becomes

$$T_e = \int_0^{i_1} \frac{\partial \lambda(\theta, i)}{\partial \theta} di \tag{2.4}$$

For these equations, the instantaneous torque can be visualized graphically: it is the work ΔW_m divided by $\Delta\theta$, where ΔW_m is evolved at constant stator current as the rotor moves through an infinitesimal displacement $\Delta\theta$. This is illustrated in Figure 2.3. During such a displacement there is an exchange of energy with the power supply, and there is also a change in the stored field energy. The constant-current constraint ensures that during such a displacement, the mechanical work done is exactly equal to the change in coenergy. This can be easily proved as follows:

In a displacement $\Delta\theta$ from A to B in Figure 2.3 at constant current, the energy exchanged with the supply is

$$\Delta W_e = S_{ABCD}$$

The change in stored field energy is

$$\Delta W_f = S_{OBC} - S_{OAD}$$

And the mechanical work done must be

$$\begin{aligned}
\Delta W_m &= T_e \Delta\theta \\
&= \Delta W_e - \Delta W_f \\
&= S_{ABCD} - (S_{OBC} - S_{OAD}) \\
&= S_{ABCD} + S_{OAD} - S_{OBC} \\
&= S_{OAB} \\
&= \Delta W^{'}
\end{aligned}$$

It can be seen that not all energy obtained from the supply is converted to mechanical work. Some of it is stored in the magnetic field. The energy stored in the magnetic field is not wasted, but it is not available for energy conversion during the motion from A to B.

If there is no magnetic saturation, the magnetization curves would be straight lines. In this case, at any rotor position θ, the coenergy and the stored magnetic energy are equal, and given by:

$$W_f = W^{'} = \frac{1}{2} L(\theta) i^2$$

Then the instantaneous torque reduces to

$$T_e = \frac{1}{2} i^2 \frac{\partial L}{\partial \theta} \tag{2.5}$$

However, it has been pointed out in [9] that, as in other types of motor, the single phase SRM suffers from starting problem. Also, there exists inevitable "blank zones" between successive torque zones, which needs sufficient load inertia to pull the motor through. There is no possibility of producing constant torque throughout one revolution. Therefore, most SRMs are multi-phase. In the multi-phase case, the torque equation becomes a summation

$$T_e = \sum_{j=1}^{m} T_{ej}$$

where T_{ej} denotes the torque generated by the jth phase, and m is the total phase number.

2.1.2 Model Equations

In general, the dynamical model of an SRM is as follows:

$$J\frac{d\omega}{dt} = T_e - B_m\omega - T_L \tag{2.6}$$

$$T_e = \sum_{j=1}^{m} T_{ej} \tag{2.7}$$

$$T_{ej} = \int_0^{i_{j1}} \frac{\partial \lambda_j}{\partial \theta} di_j \tag{2.8}$$

$$\theta_j = N_r\theta - \frac{2\pi(j-1)}{m} \tag{2.9}$$

where J is the rotor's inertia moment, B_m is the viscous friction coefficient of the rotor and T_L is the load torque; ω denotes the rotor's angular speed; $N_s = 2m$ and N_r denote the stator and rotor pole number respectively; θ denotes the rotor position with respect to starting position; θ_j denotes the rotor position with respect to the jth phase; i_j denotes the jth phase current; while T_{ej} denotes the torque generated by the jth phase.

2.2 Operating Principle

In order to guarantee that the SRM can be started at any initial rotor position, and to get smooth torque capacity per resolution, SRMs with multi-phase as well as multi-rotor-pairs are developed. The number of stator and rotor poles are generally different ($N_s \neq N_r$). Some possible combinations are: $N_s = 6$, $N_r = 4$; $N_s = 8$, $N_r = 6$; $N_s = 12$, $N_r = 10$, etc. These combinations ensure that the rotor is never in a position where the summation of the electromagnetic torque generated by each phase is zero. The larger the stator and rotor poles number, the less the torque ripple. By choosing a combination where there are two more stator poles than rotor poles, high torque and low switching frequency of the power converter can be achieved.

Figure 2.4 shows the structure of an 8/6 SRM. The following are some definitions in the literature:

Definition 1 *The rotor of an SRM is said to be at the* ***Aligned Position*** *with respect to a fixed phase if the current reluctance has the minimum value; and the rotor is said to be at the* ***Unaligned Position*** *with respect to a fixed phase if the current reluctance reaches its maximum value; otherwise the rotor is said to be at the* ***Misaligned Position****.*

For an SRM with symmetric structure, i.e. both the stator and rotor poles are distributed symmetrically, respectively, the positions defined above with respect to phase 1 are shown in Figure 2.4.

The following theorem [10] guides the manufacture and control of the SRM.

Theorem 1 *When excited, the rotor of an SRM always tends to achieve the nearest position of minimum reluctance (aligned position), which corresponds to the minimum stored energy in the system.*

Now let us take a look at how a multi-phase SRM works.

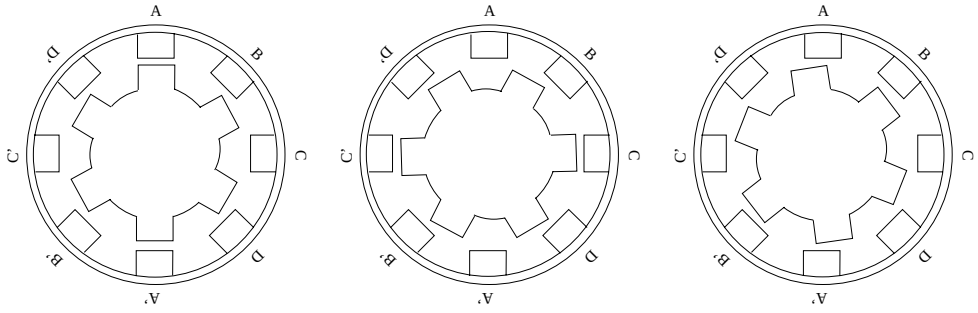

(a) (b) (c)

Figure 2.4: Structure of an 8/6 SRM:(a)Aligned Position;(b)Unaligned Position;(c)Misaligned Position

In Figure 2.5 (a), assume that at that moment only phase 1 is excited (switched on). Since at present the rotor is at the misaligned position, according to the theorem above, the rotor will turns clockwise to the aligned position in Figure 2.5 (b) because this is the nearest aligned position; If phase 1 is switched off so that the current in phase 1 is $i_{s1} = 0$ and phase 4 is switched on (excited) when the rotor reaches the aligned position in Figure 2.5 (b), the rotor will keep its clockwise rotation from its current misaligned position (Figure 2.5 (b)) to the nearest aligned position Figure 2.5 (c) with respect to phase 4; Now the rotor turns to be at the misaligned position in Figure 2.5 (c) with respect to phase 3, if phase 3 is switched on (excited) instead of phase 4, the rotor will keep clockwise rotation to Figure 2.5 (d), etc.

Therefore, the stator exciting sequence sA, sD, sC, sB, sA, ... generates clockwise rotation. For the same reason, the sequence sA, sB, sC, sD, sA, ... yields counterclockwise rotation as showed in Figure 2.6.

The speed of the SRM drive can be changed by varying the stator phase excitation sequence frequency. There is a certain relationship between them. If the fundamental switching frequency is f, then

$$f = \omega_r N_r$$

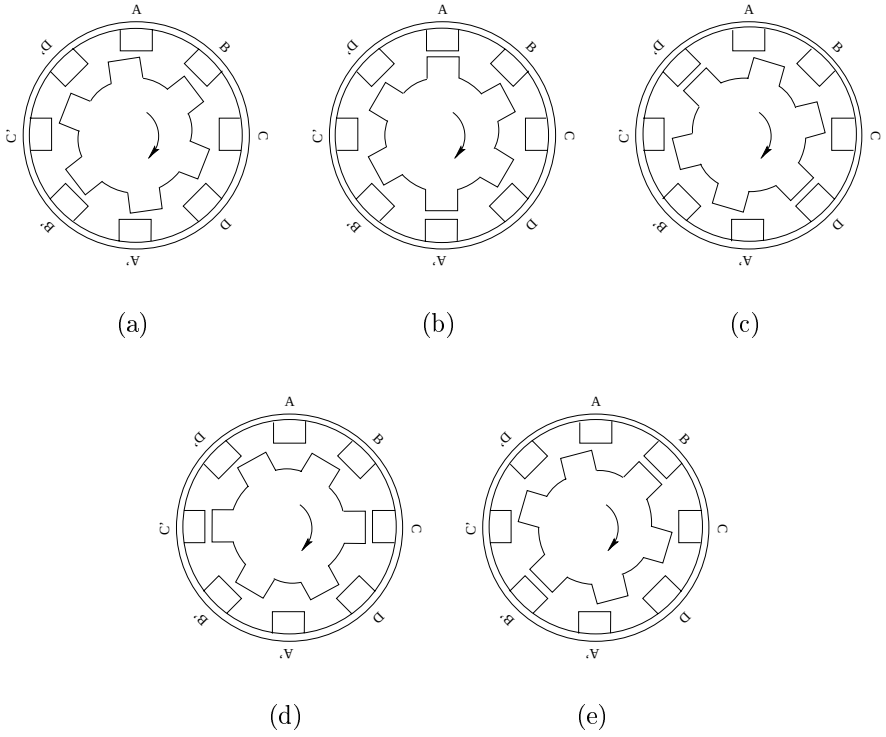

Figure 2.5: Exciting Sequence sA, sD, sC, sB, sA, ... generates Clockwise Rotation

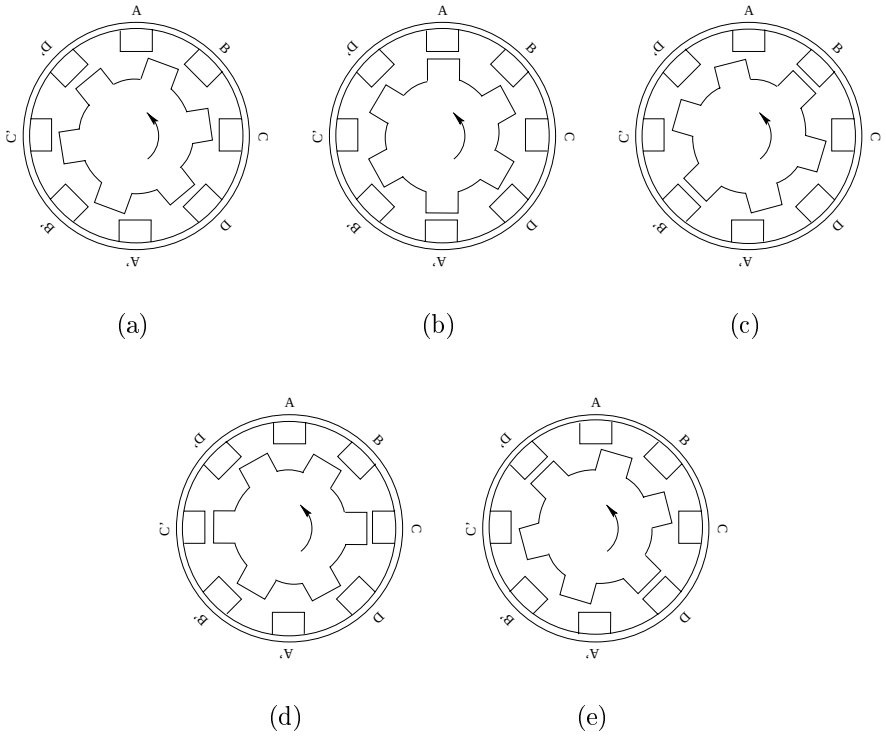

Figure 2.6: Exciting Sequence sA, sB, sC, sD, sA, ... generates Counterclockwise Rotation

where ω_r is angular rotor speed and N_r is the number of rotor poles.

As mentioned above, when current flows through one stator winding of a SRM, it is axiomatic that the torque tends to move the rotor in such a direction as to increase the inductance, until it reaches the position where the inductance has a maximum value. Provided that there is no residual magnetization in the steel, the direction of the current is immaterial (i.e. unipolar). The direction of the torque is always towards the nearest aligned position. Therefore positive torque (i.e. motoring torque) can be produced only if the rotor is between the unaligned position and the next aligned position in the forward direction. In other words, motoring torque can be produced only in the direction of rising inductance. If the rotor and stator poles are symmetric, each phase can produce unidirectional torque over only half a rotor pole-pitch. Consequently at least two phases are needed to produce unidirectional torque at all rotor position.

Thus it follows from physical consideration and also from equation (2.5) that to obtain positive (motoring) torque, the stator phase current has to be switched on during the rising inductance region of this stator phase. To obtain negative (braking) torque, the stator phase current has to be switched on during the decreasing part of the corresponding stator inductance region. It should be noted that the current in a stator phase has to be switched off before the end of the increasing inductance region for motoring mode, since in this case the current can decay to zero, and no negative torque is produced.

In brief, to control an SRM is just to control the stator excitation sequence according to the rotor position[1].

[1] As how to access the rotor position is another issue. Position sensor or position sensorless techniques can be used for this propose.

Chapter 3

Flux-Linkage Characteristics of the SRM

The double saliency structure of the SRM causes its highly nonlinear motor characteristics, which reflects completely on the flux-linkage characteristics of the motor. Compared with other types of motors, the relationship between the electrical torque and the stator currents of the SRM appears to be more complex. Generally, the generated electrical torque can be approximated by a high order polynomial of the stator currents with an order equal to or larger than two. Even for the simplest case in the linear flux region, the electrical torque is not a linear function of the stator current. That is one main reason why the control of the SRM is so challenging.

Hence, studying the motor's magnetic property is essential for proper control. In this chapter, the properties of this magnetic distribution, method of measurement and use these properties for control aims will be discussed.

3.1 Properties of the Flux-Linkage Characteristics

If both the rotor and stator poles are symmetrically distributed respectively as shown in Figure 2.4 to Figure 2.6, then it is quite easy to find that the flux-linkage λ has the following properties:

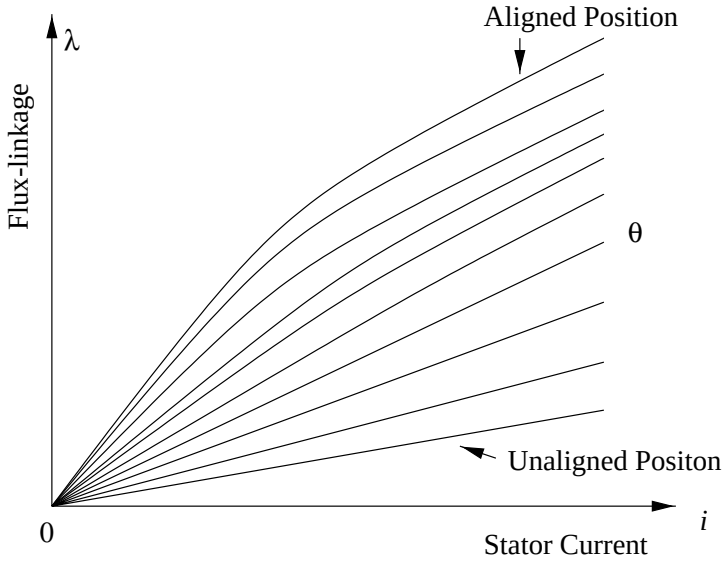

Figure 3.1: Flux-linkage Chart of the SRM

1. The flux-linkage λ of a SRM is a function of both the stator current i_j and the rotor position θ;

2. For fixed rotor position θ, the flux-linkage λ is purely a linear function of the stator current i_j only under the case when there is no saturation effect. Generally, when the stator current is under certain value (this region is called the linear flux region), the relationship between λ and i_j appears to be linear. As the stator current i_j increases, saturation occurs, which means λ is no longer a linear function of i_j. The larger i_j is, the heavier the saturating effect;

3. For fixed stator current i_j, λ is a periodic function of rotor position θ with period equals [9]

$$period = \frac{2\pi}{N_r} \tag{3.1}$$

4. If the magnetic characteristics is plotted as Figure 3.1, the flux-linkage λ is always bounded between the aligned and unaligned positions. Moreover, for the same i_j, λ is symmetric with respect to both the aligned

and unaligned position;

5. For the same larger i_j, the saturation level differs considerably for distinct rotor position θ. The closer to the aligned position, the sharper the saturation effect becomes.

3.2 Measurement of the Flux-Linkage Characteristics of the SRM

As discussed in the previous chapter, for the SRM, the rotor moves from one position to another by virtue of the characteristic of the magnetic circuit to attain a path of minimum reluctance for the flux. The torque is produced due to the tendency of the rotor poles to align with excited stator poles. The rotor poles move from an unaligned position to an aligned position. Between these two extreme positions, the torque contour follows a particular path depending on the level of excitation current. This contour represents the static torque-rotor position ($T - \theta$) characteristics of the motor. And its characteristics gives useful information on the capability of its magnetic circuit to develop average torque during normal motor operation. Hence, in order to get desired control performance, $T - \theta$ characteristics of the SRM should be determined. However, direct measurement of this characteristics requires expensive torque transducers and its associated signal processing, which is seldom adopted.

It is well known that the torque produced by an SRM is a function of the change in coenergy as the rotor moves from one position to another (see equation (2.2)). The coenergy is a function of flux linkage, exciting current and rotor position. So it is essential to determine the saturation magnetization characteristics of the SRM. This section will discuss how to measure this characteristics by experimental methods.

In this project a simple, cost effective experimental procedure and an equally simple online data processing scheme is used to obtain the flux-linkage-

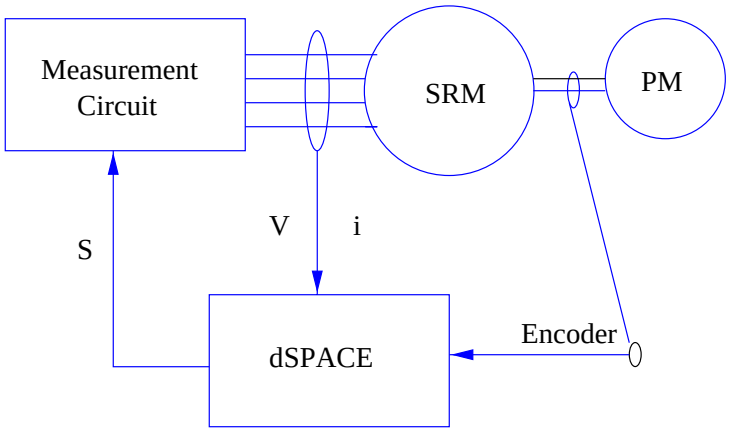

Figure 3.2: Diagram of Measuring the Flux-linkage Characteristics of the SRM

current curves at varying rotor position of the SRM. Figure 3.2 shows the diagram of the scheme.

When a voltage is added across a SRM winding, it is well known that the relationship between the current and voltage of winding is as follows:

$$V = Ri + \frac{d\lambda}{dt} \tag{3.2}$$

where R is the SRM winding resistance. So

$$\frac{d\lambda}{dt} = V - Ri \tag{3.3}$$

$$d\lambda = (V - Ri)dt \tag{3.4}$$

Thus the flux-linkage can be obtained by integrating the above equation. Using numerical processing, that is

$$\lambda = \sum_{k=0}^{N} [V(k) - Ri(k)] \triangle t \tag{3.5}$$

where $\triangle t$ is the sampling interval, $V(k)$ and $i(k)$ are the instant voltage across and current through the SRM winding at the kth sampling instant, N is the total sampling point.

Hence, in order to determine the flux-linkage it is required to sense only two electrical quantities:

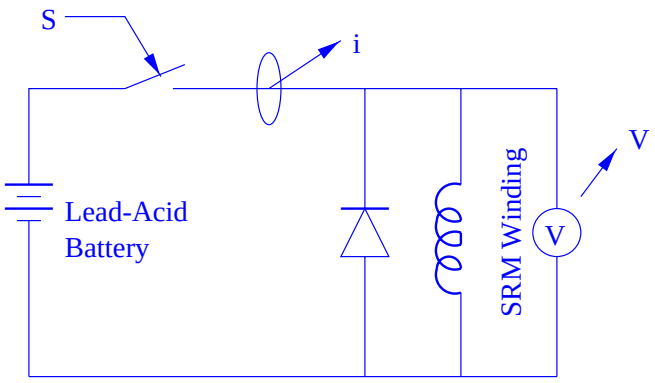

Figure 3.3: Measuring Circuit for the SRM Flux-linkage Chart

(1). the voltage appearing across the SRM winding;

(2). the current flowing through the winding starting from zero until it reaches a steady-state value higher than full load current, typically 120% of full load current.

Figure 3.3 shows the measurement circuit. In this circuit, the voltage supply resource used for the SRM winding is a Lead-Acid battery. It should be pointed out that the SRM winding resistance is usually very small, for example, only 0.1032Ω for the tested SRM in this project, which is apt to be the fatal factor limiting the use of regular power supply. For such case where resistance is small, the voltage across the SRM will not remain constant throughout the measurement period due to the poor regulation of power supply. In [11], an example is given which shows that the voltage regulation of the power supply is quite poor and the voltage drops from 60V to 20V as the current rises to steady-state value of 20A in 4ms. Therefore, an electrolytic capacitor with large capacity value is normally required to across the rectified DC. However, this will result in a series RLC circuit which generates large oscillations specially at high current level. The problems caused by voltage source regulation and current ripples due to RLC oscillations can be completely eliminated by using a pure DC source to excite the winding during the test [12]. For this purpose a set of 12V, 2AH lead acid battery is used. Depending on the resistance of

the SRM winding and the peak current required during the test, two or more batteries can be used in series.

The two electrical variables $V(t)$ and $i(t)$ needed to be sensored are measured by the inherent voltage and current sensors in the drive systems of this project. A relay controlled by the dSPACE signal S is used to excite the SRM winding momentarily so that the current reaches a steady-state value of approximately 20% more than the rated current. During the exciting period, dSPACE recorders enough data acquired by the voltage and current sensors and then processes data according to equation (3.5).

As mentioned before, the flux-linkage is a nonlinear function not only of the SRM winding current, but also of different rotor position. So on one hand, when energizing one SRM winding at certain position, the rotor has to be fixed at that position. Otherwise, the rotor will rotate due to exciting except it is at the aligned position already. For this, a permanent magnet (PM) motor is used to hold the rotor on, as shown in Figure 3.2. On the other hand, the experiment should be repeated for different rotor position in order to get enough flux-linkage characteristics information. The test is repeated only for different rotor position from aligned to unaligned position with rotor angular resolution of 2 mechanical degree. For an 8/6 SRM, the rotor pole pitch is 30° and hence the test should be conducted for fifteen discrete rotor positions. Figure 3.4 shows the diagram of this course, and Figure 3.5 shows the final experimental result.

3.3 On the Flux-Linkage Characteristics of the SRM

The first section of this chapter points out that the flux-linkage of a SRM at each rotor position is a smooth function of the stator current. However, from the above experimental results (Figure 3.5), it is quite clear that the flux-current $\lambda - i_j$ curve at each rotor position is not smooth enough. There

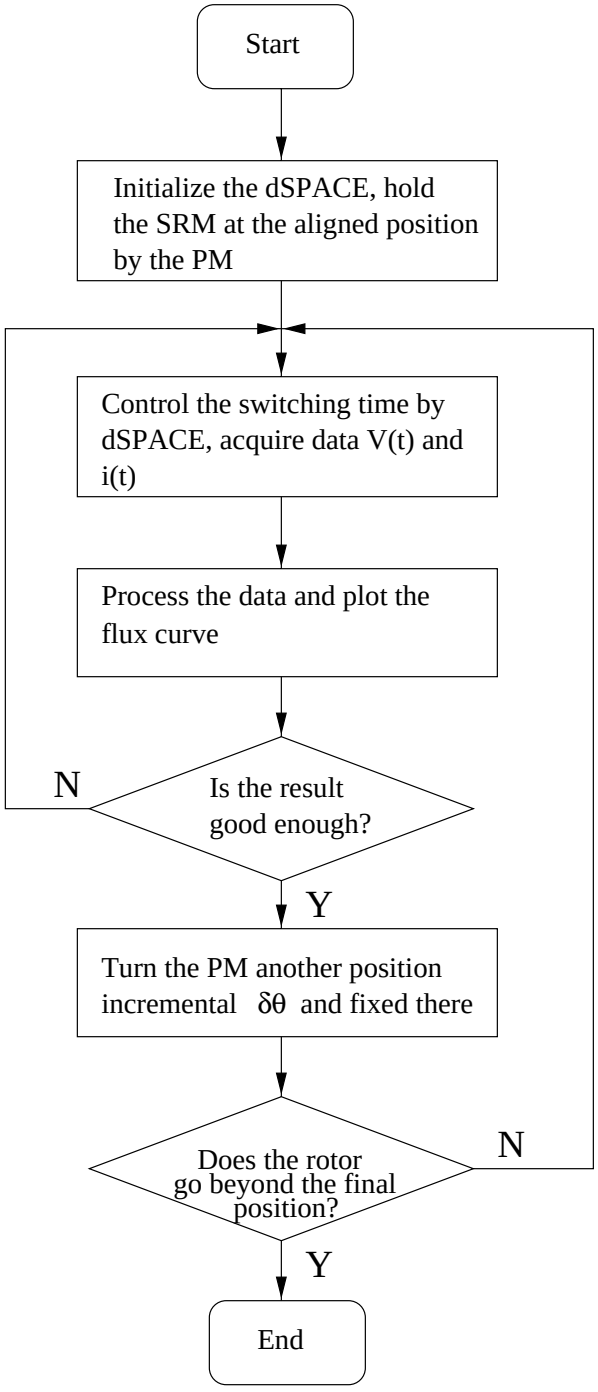

Figure 3.4: Diagram of Measuring Magnetic Chart of the SRM

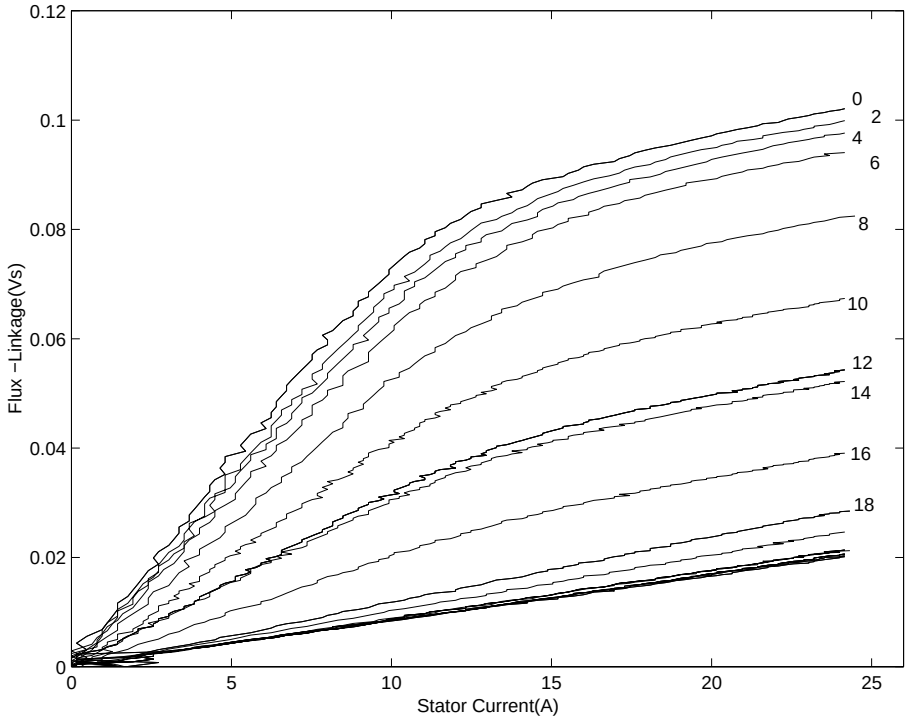

Figure 3.5: Magnetic Chart of the SRM: Experimental Result

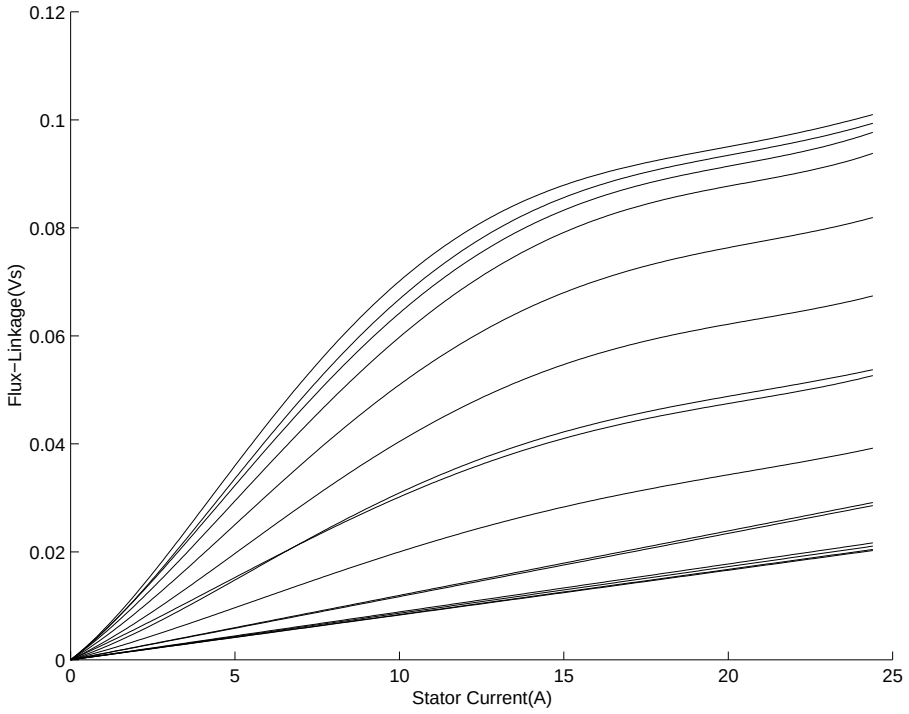

Figure 3.6: Magnetic Chart of the SRM: Polynomial Interpolation of Experimental Result of Figure 3.5

is lots of noise. So we have to filter these noisy disturbance out. In this case, standard fitting polynomial to data method can be used. Here in this project, we use a powerful tool MATLAB to smooth these curves by polynomials in least-square sense. The Matlab functions used are:

POLYFIT(X,Y,N)

POLYVAL(P,X)

Figure 3.6 is the polynomial fitting results of order 3.

On the other hand, for fixed stator currents, the flux-linkage is a smooth periodic function of rotor position. However, by experimental measurement, for each rotor pole pitch, only a finite numbers of data can be measured. For example, using the method described in previous section, only 15 flux-current curves are acquired for the 15 discrete rotor positions. As for the current, we have to make the flux being a smooth function of rotor position θ too. Theoretically, if the current controller is good enough, which requires to hold the stator current fixed as the rotor rotates to different position, we can get the $\lambda - \theta$ curves for different stator currents. Practically, to hold the rotor unmoved as the stator currents vary smoothly is much easier than to hold the stator current unchanged, when the rotor rotates to different position. Therefore, interpolation method is needed. The details are omitted in this thesis.

One of the largest challenges to control the SRM is how to make full use of the magnetic message for proper control. To operate an SRM, the commutation has to be made according the current magnetic message (or stator inductance value) and rotor position. Undoubtedly, a rotor position sensor such as position encoder can be used for the commutation needed. However, for the SRM, its inherent flux-linkage properties provide a chance to eliminate such sensoring devices. The reason is quite clear, for fixed stator current, the relationship between the flux-linkage and rotor position is quite certain. So

once we obtained the flux-linkage chart of the SRM, the rotor position and speed can be estimated by measuring other variables such as stator currents and voltages [13], [14], [15], [16], [17] and [18]. This position sensorless technology is quite essential for cost reduction.

Chapter 4

Control of the SRM in the Linear Flux Region

As mentioned in Chapter 3, how to model the SRM directly affects the complexity of the control algorithm and the final performance that can be achieved. There is lots of literature on modeling the SRM to enhance its performance. Though some of them take the saturation effect into account, it is quite convenient if the SRM is operated completely in the linear region of its flux-linkage characteristics chart because this is the simplest case. According to the flux-linkage chart of the SRM shown in Figure 3.1 and Figure 3.5, if the stator currents are small enough, this linear region operation can be guaranteed.

This chapter will focus on a four phase 8/6 SRM which is operated completely in its linear flux region.

4.1 Model in the Linear Flux Region

In this project, the SRM will be modeled under the following assumptions [19]:

A1 No Saturation Effect;

This assumption implies two cases. The first one is an ideal case. That is, the SRM is designed to be free from saturation effect. Another case is that the motor is running completely in the linear flux region, where the

stator currents are not large enough to cause saturation. This assumption makes the flux a linear function of the stator current for any fixed rotor position. In fact, in this case, the flux-linkage characteristics chart becomes a series of straight lines.

A2 Mutual inductances are ideally zero due to symmetric stator exciting;

The torque equation will be greatly simplified if the mutual inductances are zero, for the contribution of the mutual inductances to the system energy exchange will be zero too.

A3 The magnetic field distribution is sinusoidal w.r.t. the rotor position θ;

This assumption together with A1 denotes that the inductance is sinusoidal w.r.t. the rotor position θ; This modeling method solved the interpolation problem raised in Section 3.3 of Chapter 3.

A4 The saliency shape is such that no harmonics of the fundamental frequency are present for the inductance per phase.

This assumption simplifies the torque equation considerably. At the same time, it makes the controller much simple for real-time implement.

Without loss of generality, according to the assumptions above, the inductances of a 4-phase SRM can be written as [20]:

$$L_j = L_{11} - L_{22}\cos\theta_j \tag{4.1}$$

$$\theta_j = N_r\theta - \frac{\pi(j-1)}{2} \tag{4.2}$$

where j denotes the phase j, N_r is the number of rotor poles, θ is the mechanical rotor position, θ_j is the electrical rotor position with respect to phase j; $L_{11} = \frac{L_a+L_u}{2} > 0$ and $L_{22} = \frac{L_a-L_u}{2} > 0$ with L_a and L_u is defined to be the aligned and unaligned inductance respectively.

Since

$$\omega = \frac{d\theta}{dt}$$

So we can rewrite the torque equation

$$T_e = J\frac{d\omega}{dt} - B_m\omega - T_L$$

as

$$J\ \ddot{\theta}\ - B_m\ \dot{\theta}\ - T_L = T_e \tag{4.3}$$

Combining equation (2.5) with equation (4.1) and equation (4.2)

$$T_{ej} = \frac{1}{2}N_r L_{22} i_j^2 \sin\theta_j \tag{4.4}$$

Substituting into equation (2.7)

$$T_e = \sum_{j=1}^{4} \frac{1}{2}N_r L_{22} i_j^2 \sin\theta_j \tag{4.5}$$

4.2 Power Converter Topology

As indicated by its name, phase-to-phase switching in the SRM drive must be precisely timed with rotor position to obtain smooth rotation and the optimal torque output. Rotor position feedback, or the so-called "sensorless" feedback method, is needed for proper control. It is well known that this phase-to-phase switching is realized by power semiconductors. The so-called power converter topology refers to different circuit structures by power semiconductors, which can meet the SRM's switching operation mode requirement. It is well known that the power converter topology has great influence on the SRM's performance.

There are some definitions in the literature which will be used in the following discussion:

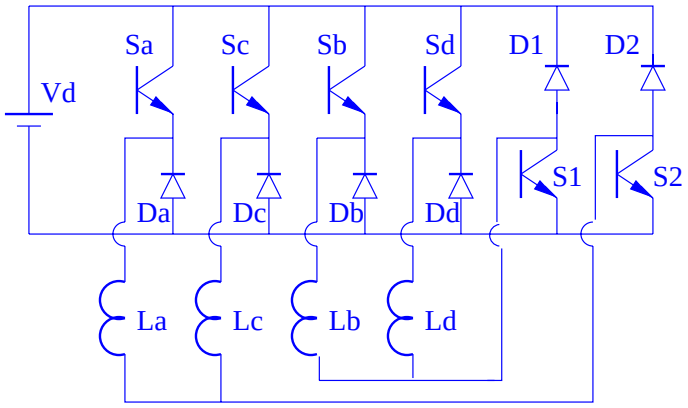

Figure 4.1: A Shared Independent Power Converter for a 4-phase SRM

Definition 2 *The rotor position where a stator current is switched on is called turn-on angle (θ_o).*

Definition 3 *The rotor position where a stator current is switched off is called turn-off angle (θ_c) .*

Definition 4 *The conduction angle (dwell angle) is defined by $\theta_d = \theta_c - \theta_o$.*

Definition 5 *The rotor position where the stator current becomes zero is called the extinction angle θ_q.*

There are many researches on power converter topology for the SRM drive. Generally speaking, there are two main classes: independent and dependent structure, according to the criterion whether it makes the control between the successive excited phases independent or not. In most cases, the dependent structure topology needs less power semiconductors than the independent structures. Also, another key difference between them is that they have different dwell angle requirements. Especially for the dependent structures, there are certain limitations on the dwell angles for proper motor control. These limitations directly affect the commutation strategy, which is the main reason why the converter topology has considerable influence on the SRM's performance.

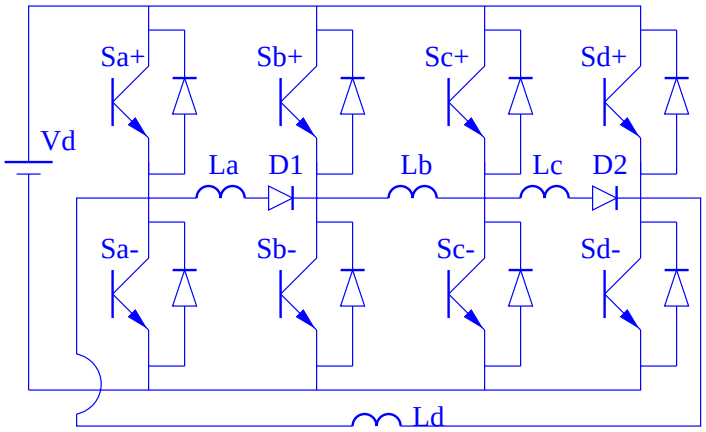

Figure 4.2: A Shared Dependent Power Converter for a 4-phase SRM

Figure 4.1 shows an independent converter structure for a 4-phase SRM. Although phase a and phase c (or phase b and phase d) share one power semiconductor S_1 (or S_2), the current or voltage control of phase a and phase c (or phase b and phase d) is independent due to the 4-phase SRM's unipolar current property and their 180° spatial phase difference. The reason will become more clear in the following.

By using the matured off-the-shelf power modules, it is quite easy to adopt different topologies for the SRM power converter without large modifications. In [21], a novel power converter topology using such off-the-shell integrated power modules is proposed. Figure 4.2 shows its circuit design. Obviously, this topology is a dependent structure. It is a fact that for this topology, the incoming excited phase and the outgoing excited phase share one bridge. For example, phase a and phase b share the bridge by S_{b+} and S_{b-}. For this reason, the dwell angle of this converter is required to be no larger than 15° for a 4-phase SRM in order to avoid short circuit of the shared bridge.

4.3 Commutation Strategy

As pointed out before, the SRM should be operated in a continuous phase-to-phase switching mode for proper motor control. The converter above by power

semiconductors is the real part to realize these switching actions. Behind the actual drives, corresponding control algorithms are needed in order to meet desired performance requirements. As a part of the control algorithm, the importance of the commutation strategy for the SRM becomes more manifest, which forms an inherent property of the SRM compared with other types of motor.

Sometimes commutation strategy is limited by the power converter topology. The commutation instant and dwell angle are directly affected by whether the control between the outgoing exciting phase and the incoming exciting independent or not. That is, apart from satisfying the SRM's own operation principle, extra requirements from the converter has to be taken into account if they exist. The difference of commutation strategy between the independent and dependent converter structure will be apparent in the following.

4.3.1 Commutation Strategy for Two-Phase-Exciting

For the independent converter structure, there is no limitation from the power converter. So the commutation strategy only needs to take care the SRM's operation principle. This strategy excites the stators as follows: for motoring mode, it excites the phases which generate positive electrical torque; for braking mode, it excites the phases which produce negative torque. For an 8/6 SRM, each time, there are always two such phases generating the same directional rotation. Figure 4.3 is the current diagram of this two-phase-exciting commutation strategy.

The commanded winding current per phase, i_{dj}, is generated from the desired torque signal $T_d(t)$, where $T_d(t)$ is designed to force the mechanical load to track the desired position trajectory, according to

$$i_{dj} = \sqrt{\frac{2}{N_r L_{22}} \left[\frac{T_d \sin\theta_j S(T_d \sin\theta_j)}{S_T} + i_{j0}^2 \right]} \tag{4.6}$$

The positive scalar design parameter i_{j0} is used to compensate the threshold

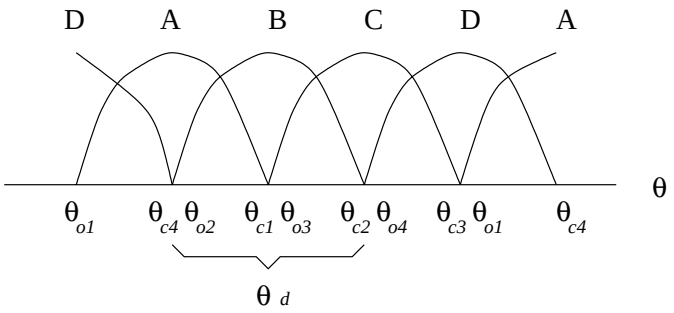

Figure 4.3: Current Diagram by two-phase-exciting for a 4-phase SRM

winding current per phase. The term $S(z)$ of the above equation is defined by the following differentiable function for arbitrary scalar z:

$$S(z) = \begin{cases} 1 - e^{-\epsilon z^2} & , z > 0 \\ 0 & , z \leq 0 \end{cases} \tag{4.7}$$

where ϵ is a positive adjustable constant which determines how closely $S(z)$ approximates the unit-step function. This function is used to simulate switch on and off behaviors of the power electronics components such as IGBT used for commutation.

The term S_T is defined as a differentiable function as follows:

$$S_T = \sum_{j=1}^{4} \sin^2 \theta_j S(T_d \sin \theta_j) \tag{4.8}$$

Given the definitions of $S(\cdot)$ and S_T above, it is easy to show that

$$\frac{T_d \sin \theta_j S(T_d \sin \theta_j)}{S_T} \geq 0 \tag{4.9}$$

However, it seems that equation (4.9) is undefined for $S_T = 0$. Given the definition of $S(\cdot)$ and S_T, it is easy to see that $S_T = 0$ when $T_d = 0$. Evaluating the left-hand side of equation (4.9) in the limit as $T_d(t)$ approaches zero yields

$$\lim_{T_d \to 0} \frac{T_d \sin \theta_j S(T_d \sin \theta_j)}{S_T} = 0 \tag{4.10}$$

for all θ; Hense, from equation (4.10), we can state that

$$\lim_{T_d \to 0} i_{dj} = i_{j0} \tag{4.11}$$

Therefore, the reference current command i_{dj} by equation (4.6) is well defined and bounded for all bounded desired torque signals and rotor positions.

Graphically, Figure 4.4 illustrates the reference current of the first phase under this commutation strategy for a 4-phase SRM with $N_r = 6$, $\epsilon = 1.0$ and $i_{j0} = 1A$. Obviously, by this commutation strategy, the desired stator current is a smooth function of T_d and θ.

To illustrate the motivation of this commutation strategy, suppose that the current loop is fast enough such that the actual current and the reference command are equal to each other, i.e.

$$i_j = i_{dj} \tag{4.12}$$

Then the torque equation can be written as

$$J\ddot{\theta} - B_m\dot{\theta} - T_L = \sum_{j=1}^{4} \frac{1}{2} N_r L_{22} i_{dj}^2 \sin\theta_j \tag{4.13}$$

Substituting equation (4.6) into equation (4.13)

$$J\ddot{\theta} - B_m\dot{\theta} - T_L = \sum_{j=1}^{4} \sin\theta_j \left[\frac{T_d \sin\theta_j S(T_d \sin\theta_j)}{S_T} + i_{j0}^2 \right] \tag{4.14}$$

Using the definition of S_T, the above equation can be simplified as

$$J\ddot{\theta} - B_m\dot{\theta} - T_L = T_d + i_{j0}^2 \sum_{j=1}^{4} \sin\theta_j \tag{4.15}$$

Expanding the summation and applying the trigonometric identity,

$$\begin{aligned} \sum_{j=1}^{4} \sin\theta_j &= \sin(N_r\theta) + \sin(N_r\theta - \frac{\pi}{2}) \\ &\quad + \sin(N_r\theta - \pi) + \sin(N_r\theta - \frac{3\pi}{2}) \\ &= 0 \end{aligned} \tag{4.16}$$

Therefore, equation (4.14) can be finally simplified as

$$J\ddot{\theta} - B_m\dot{\theta} - T_L = T_d \tag{4.17}$$

Based on this equation, it is trivial to draw conclusion that torque control, speed or position tracking can be achieved naturally.

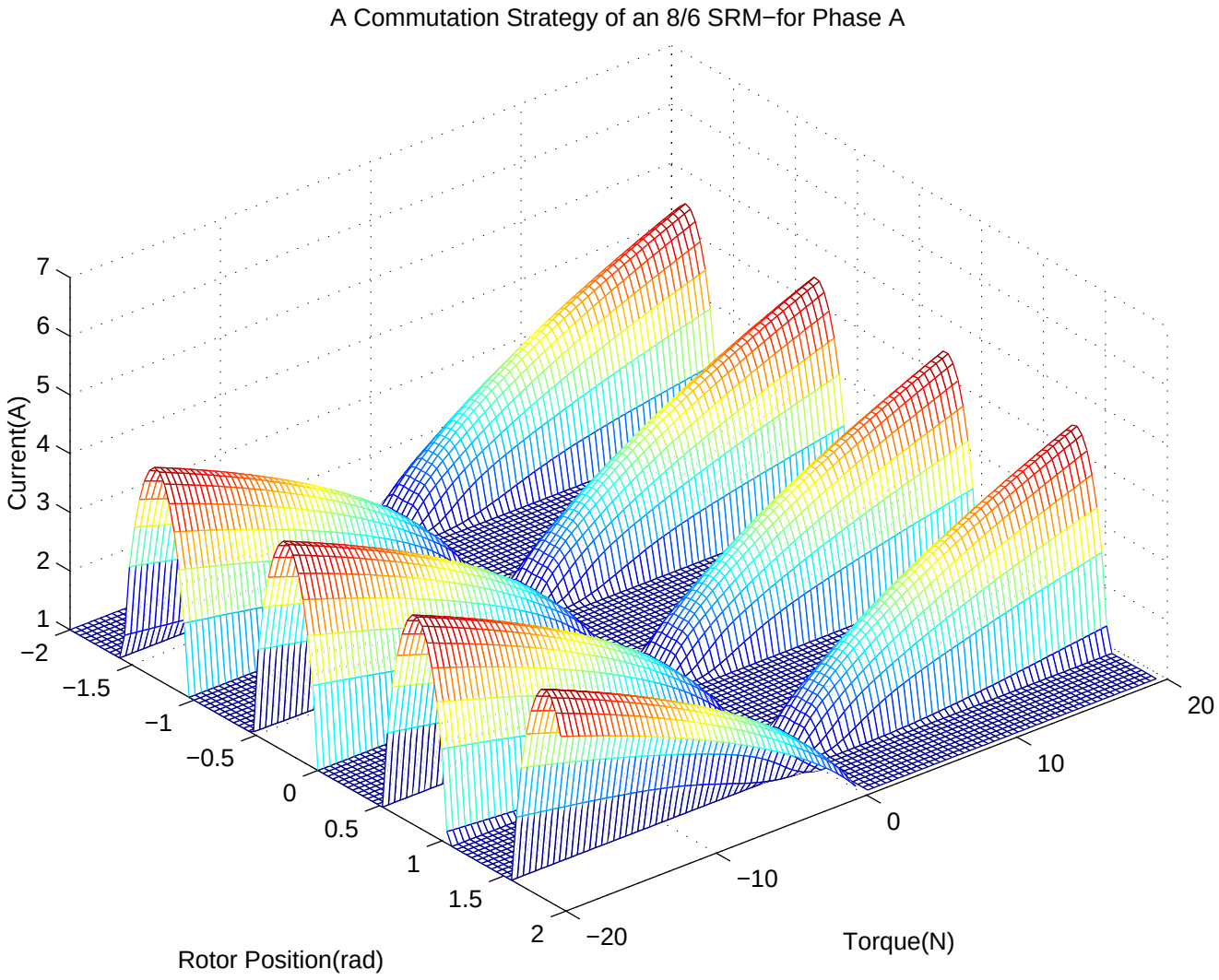

Figure 4.4: One phase Current Waveform by Two-Phase-Exciting for an 8/6 SRM

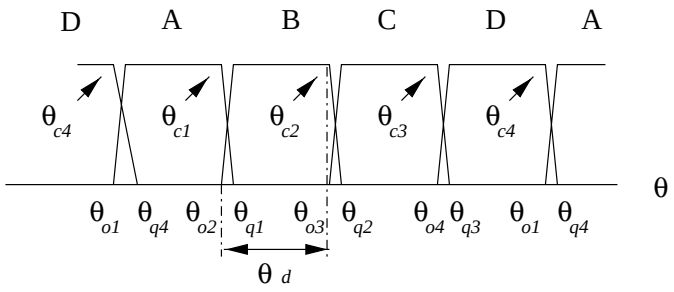

Figure 4.5: Current Diagram by Single-Phase-Exciting for an 8/6 SRM

4.3.2 Commutation Strategy for Single-Phase-Exciting

For an 8/6 SRM, although there always exists two phases generating the same directional torque, there is no need to excite both them at the same time. Also, if using the shared dependent power converter, since the outgoing exciting phase and the incoming exciting phase share power semiconductors, certain limitation arises in order to avoid short circuit. For a 4-phase SRM, the dwell angle is required to be no large than 15° for the dependent power converter structure as Figure 4.2, otherwise the shared bridge will be short circuit. In this case, only single-phase-exciting commutation strategy can be used. Figure 4.5 shows the current waveform under this limitation. Compared with Figure 4.3, it is quite clear that for independent structure, there is a period in which both the incoming and outgoing phases are excited. And this period is not permitted for the dependent power converter structure mentioned above.

Since the power converter in Figure 4.2 requires that the dwell angle is no large than 15°. From Figure 4.5 we can see that except the commutation period, there is only one phase conducting. That means except the commutation period, the only conducting phase has to provide the desired torque T_d in order to maintain the desired motion.

Since the torque generated by one phase is

$$\begin{aligned} T_{ej} &= \frac{1}{2} i_j^2 \frac{\partial L_j}{\partial \theta} \\ &= \frac{1}{2} N_r L_{22} i_j^2 \sin\theta_j \end{aligned} \tag{4.18}$$

So when phase j is excited, the following equation must be satisfied:

$$T_{ej} = T_d, \quad for \quad \theta_{oj} \leq \theta \leq \theta_{cj} \tag{4.19}$$

i.e.

$$\frac{1}{2} N_r L_{22} i_j^2 \sin\theta_j = T_d, \quad for \quad \theta_{oj} \leq \theta \leq \theta_{cj} \tag{4.20}$$

where θ_{oj} and θ_{cj} denote the turn-on angle and turn-off angle of phase j respectively, N_r and $L_{22} > 0$ are defined in the previous section.

From equation (4.20), it is quite clear that once a phase is excited, it has to satisfy the condition that $\sin\theta_j$ and T_d should have the same sign so as to provide the desired torque.

So the commanded winding current per phase i_{dj} can be generated from the desired torque signal $T_d(t)$ as follows:

$$i_{dj} = \sqrt{\frac{2}{N_r L_{22}} \left[\frac{T_d}{\sin\theta_j} + i_{j0}^2 \right]}, \theta_{oj} \leq \theta \leq \theta_{cj} \tag{4.21}$$

The positive constant i_{j0} is still used to compensate the threshold winding current per phase.

Obviously, the commanded reference current i_{dj} in equation (4.21) is not defined for all θ_j. We know that, the reference current i_{dj} should be zero if the phase j is not excited. That is

$$i_{dj} = \left\{ \begin{array}{ll} \sqrt{\frac{2}{N_r L_{22}} \left[\frac{T_d}{\sin\theta_j} + i_{j0}^2 \right]} & , \theta_{oj} \leq \theta \leq \theta_{cj} \\ 0 & , otherwise \end{array} \right\} \tag{4.22}$$

It should be pointed out that equation (4.22) will be undefined if the turn-on angle and turn-off angle are not properly chosen. One basic criterion is that they have to satisfy the condition that $\sin\theta_j$ and T_d should have the same sign if phase j is excited. The coming section will discuss how to choose these angles.

4.4 Performance Optimization for Single-Phase-Exciting

In this section, we will discuss how to choose the turn-on angle and turn-off angle properly based on the dependent power converter topology as shown in Figure 4.2 so that the performance can be optimized.

It is a fact that the commutation instant has essential influence on the SRM's performance. When and how to commutate from one phase to another directly determines the stator current wave form, the motor's power efficiency, torque ripple and dynamic performance.

Since the dependent power converter topology does not make incoming and outgoing phases completely independent. It requires the dwell angle for an 8/6 SRM to be no larger than 15°. However, equation (4.20) shows that when phase j is excited, it can generate the motor(or brake) torque for one rotor pitch which is one half of its inductance period. That is the independent structure case where $\theta_d = 30°$ for a 4-phase SRM as shown in Figure 4.3.

Since the dwell angle $\theta_d \leq 15°$, from equation (4.2), it is easy to find that the turn-on angle θ_{oj} satisfying equation (4.20) is not unique. For example, conducting phase one ($j = 1$) to generate positive T_d, in one electrical cycle, θ_{o1} can be any value between $(0, 15°)$ if $\theta_d = 15°$. The turn-on angle is unique only when $\theta_d = 30°$ for a 4-phase SRM. The rest of this section investigates these values to find the best turn-on angles for the SRM.

Multiply both side of equation (4.20) by V_d^2,

$$\frac{1}{2}N_r L_{22} V_d^2 i_j^2 \sin\theta_j = V_d^2 T_d$$

$$k_1 (V_d i_{dj})^2 \sin\theta_j = V_d^2 T_d = k_2$$

i.e.

$$k_1 P^2 \sin\theta_j = k_2 \tag{4.23}$$

where $V_d > 0$ is DC voltage supplied to the SRM and $P = V_d i_{dj}$ is the instantaneous power. Therefore the average power of phase j for its conducting period per cycle is

$$\overline{P} = \frac{1}{N_r\theta_d}\int_{N_r\theta_{oj}}^{N_r\theta_{cj}} \sqrt{\frac{k_2}{k_1 \sin[\theta - 90^\circ \times (j-1)]}}\, d\theta \tag{4.24}$$

For a fixed dwell angle $\theta_d \neq 0$, equation (4.24) can be written as a function of the turn-on angle θ_{oj}

$$\begin{aligned} \overline{P} &= \frac{1}{N_r\theta_d}\int_{N_r\theta_{oj}}^{N_r(\theta_{oj}+\theta_d)} \sqrt{\frac{k_2}{k_1 \sin[\theta - 90^\circ \times (j-1)]}}\, d\theta \\ &= f(\theta_{oj}) \end{aligned} \tag{4.25}$$

For simplicity, the following only discuss the case for $j = 1$:

Differentiate $f(\theta_{o1})$ with respect to θ_{o1}

$$\frac{df}{d\theta_{o1}} = \sqrt{\frac{k_2}{k_1 \sin(N_r\theta_{o1} + N_r\theta_d)}} - \sqrt{\frac{k_2}{k_1 \sin(N_r\theta_{o1})}} \tag{4.26}$$

$$\begin{aligned} \frac{d^2 f}{d\theta_{o1}^2} &= \frac{N_r k_2 \cos(N_r\theta_{o1})}{2k_1 \sin^2(N_r\theta_{o1})}\sqrt{\frac{k_1 \sin(N_r\theta_{o1})}{k_2}} \\ &\quad - \frac{N_r k_2 \cos(N_r\theta_{o1} + N_r\theta_d)}{2k_1 \sin^2(N_r\theta_{o1} + N_r\theta_d)} \\ &\quad \cdot \sqrt{\frac{k_1 \sin(N_r\theta_{o1} + N_r\theta_d)}{k_2}} \end{aligned} \tag{4.27}$$

Now let the first derivative be zero

$$\sqrt{\frac{k_2}{k_1 \sin(N_r\theta_{o1} + N_r\theta_d)}} - \sqrt{\frac{k_2}{k_1 \sin(N_r\theta_{o1})}} = 0 \tag{4.28}$$

$$\sin(N_r\theta_{o1}) = \sin(N_r\theta_{o1} + N_r\theta_d)$$

If $T_d > 0$, that is $k_2 > 0$, then

$$N_r\theta_{o1} + N_r\theta_{o1} + N_r\theta_d = 180^\circ$$

$$\theta_{o1} = \frac{90^\circ}{N_r} - \frac{\theta_d}{2}$$

Considering that θ_{o1} is periodic [9], so

$$\theta_{o1} = \frac{k \times 360^\circ + 90^\circ}{N_r} - \frac{\theta_d}{2}, k = 0, \pm 1, \pm 2, \cdots \tag{4.29}$$

Use this solution for equation (4.27)

$$\begin{aligned} \frac{d^2 f}{d\theta_{o1}^2} &= \frac{N_r k_2 \cos(N_r\theta_{o1})}{k_1 \sin^2(N_r\theta_{o1})} \sqrt{\frac{k_1 \sin(N_r\theta_{o1})}{k_2}} \\ &> 0 \end{aligned}$$

If $T_d < 0$, that is $k_2 < 0$, then

$$N_r\theta_{o1} + N_r\theta_{o1} + N_r\theta_d = 360^\circ + 180^\circ$$

$$\theta_{o1} = \frac{180^\circ + 90^\circ}{N_r} - \frac{\theta_d}{2}$$

Make it periodic as above

$$\theta_{o1} = \frac{k \times 360^\circ + 180^\circ + 90^\circ}{N_r} - \frac{\theta_d}{2}, k = 0, \pm 1, \pm 2, \cdots \tag{4.30}$$

Substituting equation (4.30) into equation (4.27):

$$\begin{aligned} \frac{d^2 f}{d\theta_{o1}^2} &= -\frac{N_r k_2 \cos(N_r \theta_{o1})}{k_1 \sin^2(N_r \theta_{o1})} \sqrt{\frac{k_1 \sin(N_r \theta_{o1})}{k_2}} \\ &> 0 \end{aligned}$$

Therefore, except for the trivial case $T_d = 0$, equation (4.29) and (4.30) give the smallest average power for positive and negative torque command respectively when phase one ($j = 1$) is excited. By the same procedure, it is easy to find that for phase j, the proposed turn-on angle is:

For $T_d > 0$

$$\theta_{oj} = \frac{k \times 360^\circ + j \times 90^\circ}{N_r} - \frac{\theta_d}{2}, k = 0, \pm 1, \pm 2, \cdots \tag{4.31}$$

For $T_d < 0$

$$\theta_{oj} = \frac{k \times 360^\circ + 180^\circ + j \times 90^\circ}{N_r} - \frac{\theta_d}{2}, k = 0, \pm 1, \pm 2, \cdots \tag{4.32}$$

Hence, if commutation a 4-phase SRM according to equation (4.31) and (4.32) based on the power converter topology shown in Figure 4.2, the highest power efficiency will be achieved.

Moreover, if the DC voltage supplied to the SRM is stable enough, that is $V_d = const$, from the analysis above, the smallest average power is equivalent to the smallest average stator current, for they are only different by a positive constant.

4.5 Closed-Loop System

Figure 4.6 is the general diagram of the SRM with closed loop speed control. The core loop is the torque controller. In position or speed control application an outer loop is added to the torque controller, with a fast inner current loop

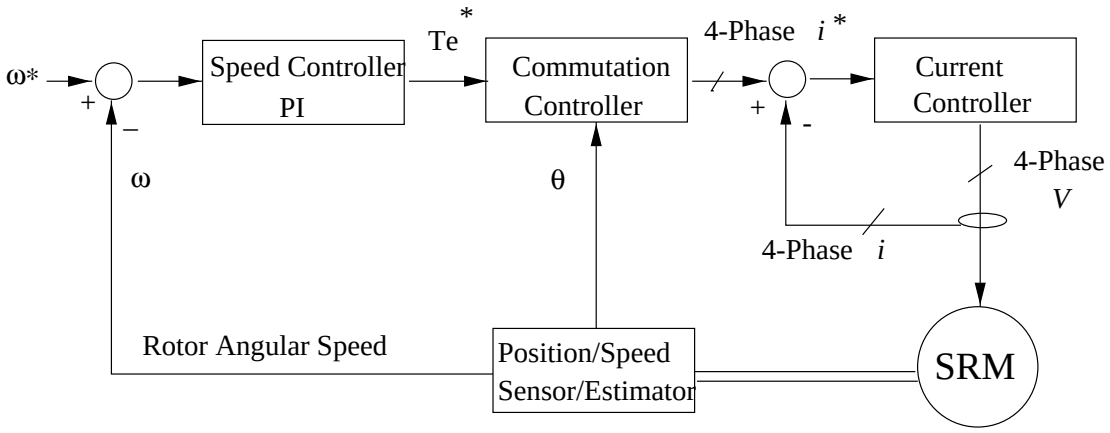

Figure 4.6: Diagram of the Closed-Loop System

that can be regarded as creating impressed currents to the stator windings necessary to achieve the desired torque specified by the outer loops. It has been pointed out in [20], there appears to be universal agreement that this structure is the most effective control scheme for electrical drives.

The innermost current loop is implemented by a current tracker, which consists of current controller, power converter, the stator windings of the SRM and current sensoring devices for feedback control. The performance of this loop has a critical influence on the whole system, especially for the current model discussed in this chapter. Usually, there are three kinds of current controllers [23]: PI controller, hysteresis controller and a hybrid structure by the combination of the first two. In this project, a PI current controller is used for its simplicity. Also, the power converter and the current sensoring device will be discussed in the next chapter.

The commutation controller and speed controller are realized by the dSPACE controller which will be discussed in detail later. These loops are the core of the control algorithm. The previous section showed the commutation strategies already. The only part left to be considered is the speed controller. There are many choices for this controller, such as PI controller, two degree of freedom controller, robust controller, fuzzy controller, adaptive controller, artificial

neutral network controller and so on. Undoubtedly, they can achieve different system performances. In this thesis, the speed loop adopted a PI controller as the current controller for the same reason.

As pointed out by theorem analysis and Figure 4.6, the speed or position of the rotor need feedback for proper control. This can be done by sensoring device or estimation. The position sensorless technology uses such estimators for speed and position feedback. In this project, we use a position encoder for this purpose.

4.6 Starting Problem

Like the PM, starting problem of the SRM has to be considered in order to get the desired performance. Although an 8/6 SRM is designed so that it can start at any initial position [9], it can not rotate smoothly if the start problem is not correctly solved [25]. The reason is quite clear when studying its operation principle. The phase-to-phase switching in the SRM drive must be precisely timed with rotor position to obtain smooth rotation and the optimal torque output. Therefore, when starting the motor, the current rotor position has to be exactly identified. That is, we have to know exactly where the rotor poles is aligned with respect to the exciting phase. Otherwise, proper commutation can't be guaranteed. Consequently, wrong commutation will lead to counter-desired torque blocking desired motion, which can even stop the rotor's rotation.

In this project, a novel starting scheme is proposed. The key idea of this method is to align one pair of rotor poles to one phase by a certain exciting current. And then use this position as reference position for the commutation. By doing so, the desired starting performance can be achieved.

When starting, exciting one phase with constant current for some period, for example, say phase B. As discussed before, the rotor will align to phase B along the shortest path under this exciting, if the generated torque is large

enough to overcome the rotation friction. How to choose the constant current value and conducting period is not trivial. This exciting stator current should be able to align the rotor to the nearest exciting phase. It has to be able to produce such a torque to overcome the load and friction. While the conducting period should be long enough to guarantee the finish of this aligning action. If the exciting period is too short, the rotor can't reach the aligned position due to load and friction; On the other hand, if the exciting period is too long, it will waste energy.

A value two thirds of the rated current of the SRM is chosen as the initial exciting current. If this current is large enough, the rotor will be able to move to the nearest aligned position. As discussed before, the rotor will rotate once there is one phase excited unless the rotor is already at the aligned position with respect to that phase. Also, it will hold the rotor at the aligned position if no other phases excited sequentially. When the rotor keeps stationary after the exciting, there are two cases for phenomenon: the exciting current is not large enough to generate rotation; the rotor itself is at the aligned position already. Obviously, we have to differentiate them for proper starting.

Hence, an additional method is needed. After exciting one phase (say phase B), if the rotor remained stationary, then move the exciting current to its adjacent phase (phase A or C) for the same period. If the rotor still keep unmoved, it means that the exciting current is too small to align the rotor and need to be increased. Otherwise, it means the rotor is already at the aligned position with the previous exciting phase (phase B). In this case, the current aligned position can be taken as an initial reference position for commutation. In the cases where the load is unknown, this tuning procedure can be repeated.

In this project, we start the 8/6 SRM as following steps:

Step 1. Choosing the exciting current value according to the discussion above;

Step 2. Exciting phase B with the constant current. If the rotor remained stationary, go to step 3; Otherwise, keep the exciting of this phase until the

rotor stops;

Step 3. Excite phase A with the same constant current. If the rotor keep stationary, increase the exciting current and go back to step 2; Otherwise go to step 4 when the rotor stops rotation;

Step 4. Take the current aligned position as the initial reference position. That is, the initial relationship between the stator and the rotor is that the rotor is at the aligned position with respect to phase A. Reset the position encoder if it belongs to an increasing type. And begin the control algorithm.

Chapter 5

Experiments Setup

As described in the previous chapter, the whole system consists of different controllers, a SRM, current and position sensing devices. In this chapter, the details of design, construction and assembly of the test bed will be discussed.

5.1 Controller—dSPACE

In order to implement the control algorithm so as to control the SRM, a proper controller is needed. dSPACE is one which acts as the interface between the host PC and controller.

dSPACE is the acronym for Digital Signal Processing and Control Engineering Co. Ltd. dSPACE is the controller product.

dSPACE Prototyper is a flexible development system that lets users test their controller designs on the real controlled system directly in Simulink and SystemBuild models without programming at all. Users can also integrate their existing controllers with the bypass method. They can choose from a wide range of software/hardware components to set up their own personal dSPACE Prototyper. The dSPACE Prototyper consists of two parts: Software Prototype and Hardware Prototype. For example, the Software Prototype used in this project is MATLAB/Simulink, while the Hardware Prototype is a DS1102 DSP Controller Board.

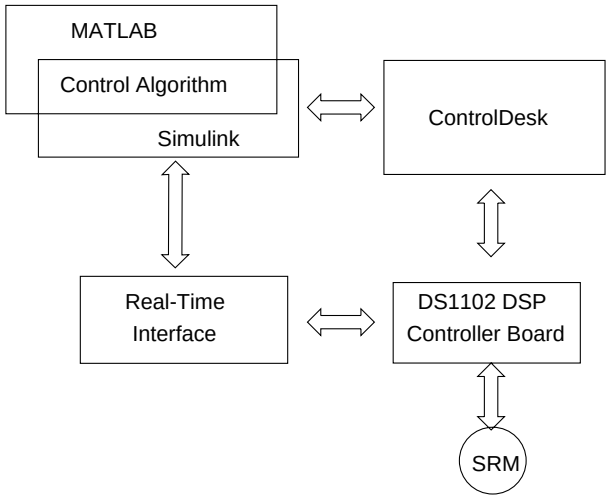

Figure 5.1: Diagram of dSPACE Controller

Rapid control prototyping is used to develop and optimize new control concepts on a real system. Design tools such as MATLAB/Simulink enable different users to design their own controllers directly in the block diagram. Real-time code is generated from the block diagram and automatically implemented on flexible prototyping hardware. In closed loop, users can change parameters online, record time histories in real time, and run through automation scripts in a development phase where the costs for corrections are still minimal.

Figure 5.1 shows how this controller works. Users program their control algorithms using MATLAB/Simulink. And after compiling, these algorithms will be downloaded to the DS1102 DSP controller board by means of a real-time workshop. Once the algorithm has been downloaded, the DS1102 will handle the control of its targets such as the SRM in this project, as well as communication with host PC. At the same time, users can use software ControlDesk to tune the control parameters such as PID parameters online, and supervise experimental results online and record data online as well.

Figure 5.3 is the DS1102 DSP Controller Board and Figure 5.2 shows its architecture. Its technical details are as follows:

Figure 5.2: DS1102 DSP Controller Board

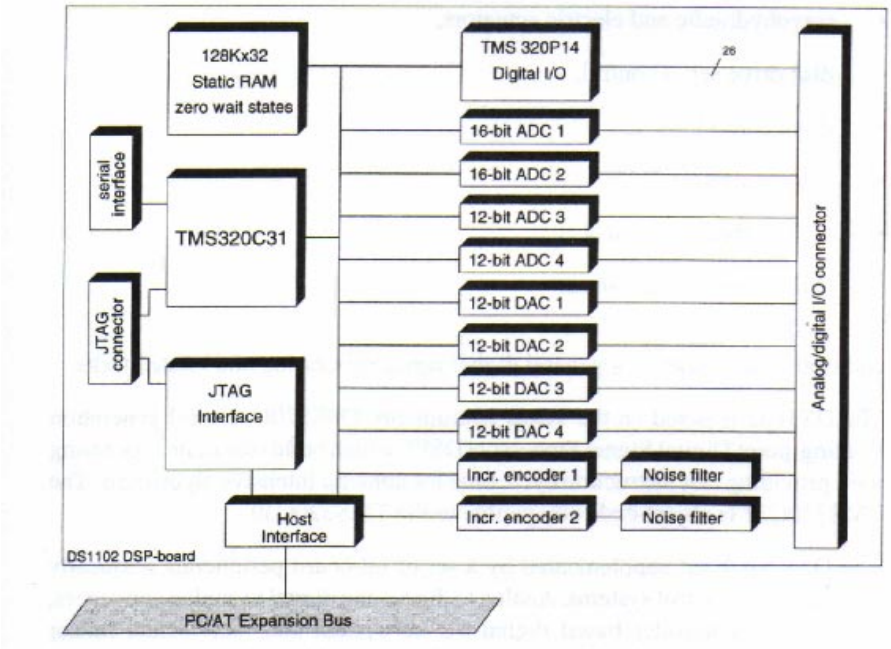

Figure 5.3: Architecture of DS1102 DSP Controller

Processor	• TI's TMS320C31 floating-point DSP • 60MHz clock rate, 33.3ns cycle time • 8-MBaud serial interface • 4 external interrupts
Memory	• 128K×32-bit RAM, zero wait states • 2K×32-bit on-chip RAM
Analog Input	• 2 parallel 16-bit channels, $4\mu s$ conversion time • 2 parallel 12-bit channels, $1.25\mu s$ conversion time • Simultaneous sample & hold • $\pm 10V$ input voltage range • >80 dB (16 bit)/65 dB (12 bit) signal-to-noise ratio
Analog Output	• 4 parallel 12-bit channels • $4\mu s$ typical settling time • $\pm 10V$ output voltage range
Digital I/O	• Programmable digital-I/O subsystem based on TI's 25MHz TMS320P14 DSP • 16 digital I/O lines(bit-selectable) • Capture/compare unit with 8 channels (2 in, 4 out, 2 in/out) • PWM generation on up to 6 channels (40 ns resolution) • User interrupt
Incremental Encoder Interface	• Two parallel input channels for two phase lines and one index line each • Fourfold pulse multiplication • 8.3 MHz max. count frequency • Noise filter • 24-bit position counter
Physical Characteristics	• Power supply 5V, 1.5A and ±12V, 100mA • Requires half-length 16-bit ISA slot • 62-pin female high-density Sub-D connector

5.2 Power Converter (PWM drive)

Power converter is the core component of a current controller. The performance of this PWM drive will directly affect the overall performance of the whole system.

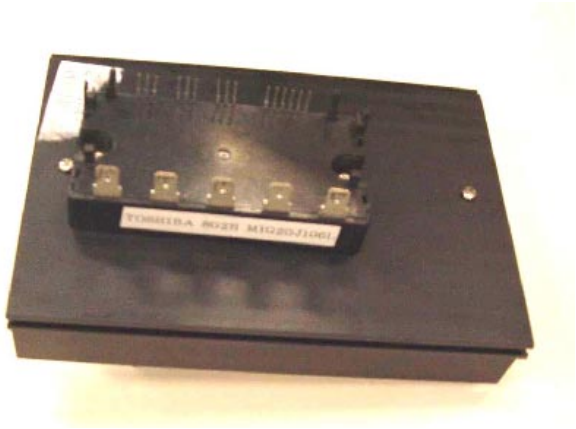

Figure 5.4: IGBT Module

The main components of a four phase PWM driver are the eight power transistors. In our hardware prototype, we adopt eight IGBTs (Insulated Gate Bipolar Transistor) because of its high voltage rating, high current rating, low leakage current, high input impedance and fast turn on/off speed [19]. In this research, two intelligent power modules from Toshiba Inc., which has advanced features such as overheat and overcurrent protection. Also, it is flexible enough to construct different converter topologies for the SRM without much changes. For an example, for the topologies discussed in the previous Chapter. Figure 5.4 shows a real physical power module.

5.3 Current Sensing Devices

The stator current of each phase needs to be measured for feedback control, especially for the current loop.

In this project, Hall effect current sensing devices from LEM Inc. were used. This type of sensing device not only has the advantage of complete isolation from sensed signal, but also is easy to implement.

The technical specification of the 4-phase channel current sensor is as follows:

1. current sensing range of each channel: 0A to ±50A adjustable

2. frequency range of each channel: DC to 100KHz

The following Figure 5.5 is the frequency response of each channel:

5.4 Position Sensor and Velocity Estimation

5.4.1 Position Sensor

From Chapter 4, it is quite clear that accurate position information of the rotor is very important for the control of the SRM, because the right commutation sequences are decided based on accurate rotor position.. Therefore, a 2048 pulse/rev optical encoder by BEI corp. is used in this project. What is more, combining with a HP optical decoder IC, 4×2048 pulse/rev is achieved. Figure 5.6 shows the actual optical encoder.

5.4.2 Velocity Estimation

The rotor angular velocity can be estimated using the following form

$$\omega \approx \frac{\theta(k) - \theta(k-1)}{T}$$

where $\theta(k)$ is the current position sample, $\theta(k-1)$ is the previous position sample and T is the sampling period.

Obviously, the resolution of this estimator is

$$\triangle\omega = \frac{60}{2048 \times 4T}(RPM)$$

For example for the sample frequency $f = 2KHz$ used in this project

$$\triangle\omega = \frac{60}{2048 \times 4 \times 0.0005} = 14.648(RPM)$$

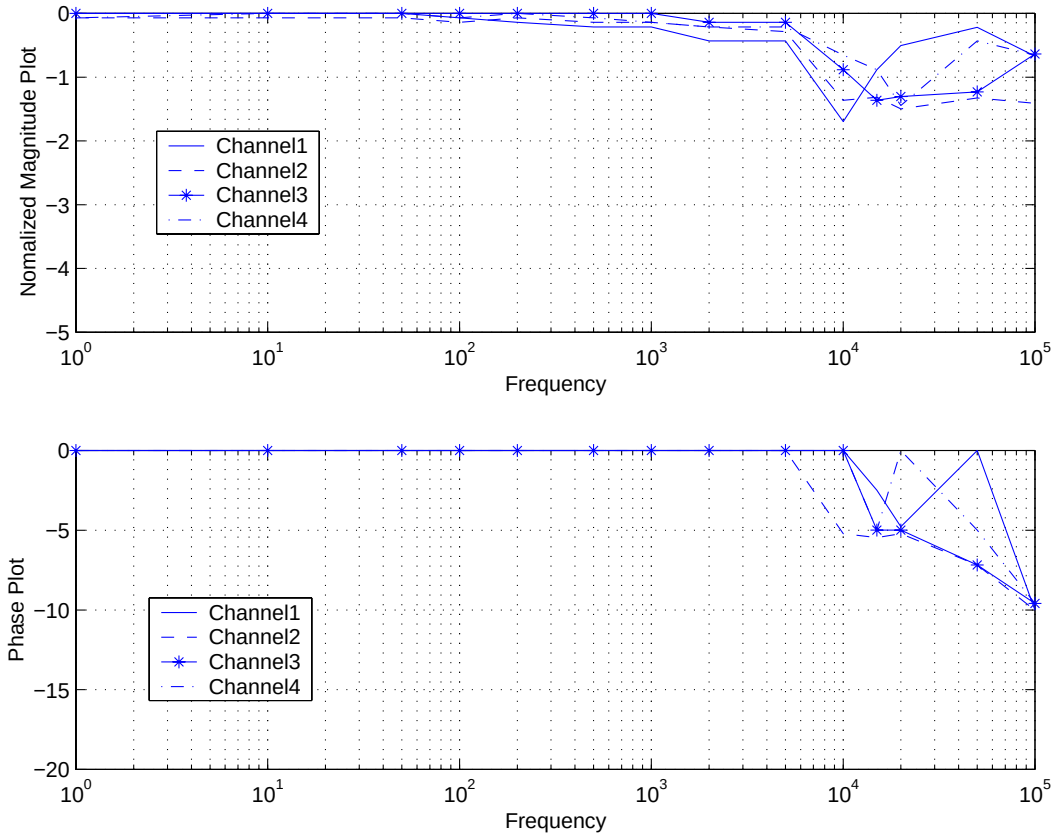

Figure 5.5: Frequency Response of the Current Sensors

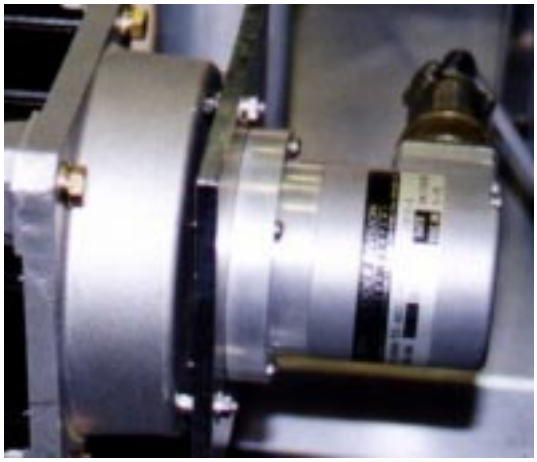

Figure 5.6: The BEI Position Encoder

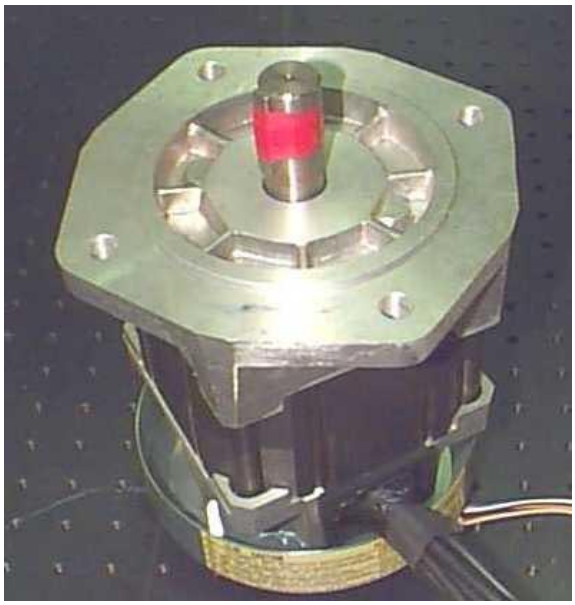

Figure 5.7: the SRM Used

5.5 The SRM

A DENSEI RA165187-001-001 8/6 SRM by Nippon Electric Industry Co. Ltd is used in this project. Figure 5.7 shows the SRM used in this project and the technical specification are as follows:

Rated Power	$1.5KW(2HP)$
Rated Torque	$2.5Nm$
Rated Speed	$6,000RPM$
Max Speed	$10,000RPM$
Number of Phases	$m = 4$
Number of Stator Poles	$N_s = 8$
Number of Rotor Poles	$N_r = 6$
Aligned Phase Inductance	$L_a = 4.68mH$
Unaligned Phase Inductance	$L_u = 0.737mH$
Phase Resistance	$R = 102.3m\Omega$
Inertia	$J = 0.0009973Kg \cdot m^2$
DC Voltage Supply	$V_d = 150V$

Chapter 6

Experimental Results

In this chapter, experimental results will be demonstrated.

The following notes refer to all experimental results:

Note 1: All experimental results were measured under zero load for simplicity;

Note 2: Except for the commutation strategies, all other control parameters have the same value for comparison. They used exactly the same speed controller and current controller with the same PI tuning value, respectively;

Note 3: For the single-phase-exciting method, the dwell angle is adopted to be 15°;

Note 4: For non-optimized single-phase-exciting, the turn-on angle of phase j is chosen as follows:

For the motoring mode

$$\theta_{oj} = \left\{ \theta \mid \max_{\theta} \frac{\partial L_j}{\partial \theta} \right\}$$

which is corresponding to the middle point of the rising inductance period.

For the braking mode

$$\theta_{oj} = \left\{ \theta \mid \min_{\theta} \frac{\partial L_j}{\partial \theta} \right\}$$

which is corresponding to the middle point of the decreasing inductance period.

6.1 Experimental Results

Figure 6.1 to Figure 6.5 shows the steady-state current waveforms of phase A and phase B of the 8/6 SRM without any load using different exciting methods. Figure 6.1 and Figure 6.2 are the results by two-phase-exciting at $\pm 1000RPM$ respectively; Figure 6.3 to Figure 6.5 are the single-phase-exciting results; Figure 6.3 and Figure 6.5 are results using optimized one phase exciting method at $\pm 1000RPM$ respectively, while Figure 6.4 is the non-optimized single-phase-exciting result.

Figure 6.9 and Figure 6.10 are the current waveforms at low speed case $100RPM$ by optimized and non-optimized single-phase-exciting method.

Speed tracking capacities of the three commutation strategies are tested from different sides. Steady-state error, dynamical response and curve tracking ability are compared at a wide speed range. Figure 6.6 to Figure 6.8 show the steady-state speed at $1000RPM$; Figure 6.11 to Figure 6.17 show the speed comparison when tracking a square wave speed command with low and high speed respectively; While Figure 6.18 to Figure 6.21 show the cases when tracking a trapezoid speed command.

6.2 Conclusion

From the experimental results, we can make conclusions as follows:

1. Figure 6.1 and Figure 6.2, Figure 6.3 and Figure 6.5 show the principle to operate a SRM. Exciting sequences $sA, sB, sC, sD, sA, ...$ and $sA, sD, sC, sB, sA, ...$ generate different directional rotation;

2. As pointed out in chapter 2, the fundamental commutation frequency is proportional to the rotor angular speed ($f = \omega_r N_r$). This principle can

be viewed clearly by reading the conducting time of each phase from the current waves at $100RPM$ and $1000RPM$ in these current figures;

3. As pointed out before, by two-phase-exciting, there is always a period in which there are two phases excited at the same time. The large current waveform overlaps between phase A and phase B in Figure 6.1 and Figure 6.2 prove this point;

4. For single-phase-exciting, each time there is only one phase excited. Reflecting on the current waveform, the overlap period between the incoming and outgoing phases is much shorter or even vanishes. This period depends on how fast the outgoing phase current can vanish to zero after removing the excitation. Figure 6.3 to Figure 6.5, Figure 6.9 and Figure 6.10 show this fact;

5. Among the three exciting methods used, the current peak value per phase by two-phase-exciting is the smallest one. The optimized single-phase-exciting method is in the middle, while the non-optimized single-phase-exciting method has the highest current peak value. Figure 6.1 and Figure 6.5 shows the steady-state current per phase by two-phase-exciting at $1000RPM$ has a peak value of around $1.5A$, the optimized single-phase-exciting (Figure 6.3 and Figure 6.5) is $1.8A$ and the non-optimized single-phase-exciting (Figure 6.4) $6A$ which is far larger than the other two at the same speed and load level. The difference between the two-phase-exciting and the single-phase-exciting is easy to understand. Since there are two phases providing the energy needed each time, so the two-phase-exciting can utilize a relatively smaller stator current than the single-phase-exciting;

6. For the single-phase-exciting method, the current waveform per phase by optimized and non-optimized methods differs a lot. Figure 6.9 and Figure 6.10 show the distinct difference of the current waveforms at $100RPM$,

which proved the potential of the proposed method. Since when the supplied *DC* voltage to the SRM is kept as a constant, optimizing the system power is equivalent to optimizing the stator current;

7. In quite a large speed range, the optimized single-phase-exciting has almost the same speed tracking capacity as the two-phase-exciting method. Their steady-state speed error (Figure 6.6 and Figure 6.7) and dynamical responses (Figure 6.11 and Figure 6.12, Figure 6.14 and Figure 6.15, Figure 6.18 and Figure 6.19) are almost the same;

8. Non-optimized single-phase-exciting is the worst commutation strategy under the same condition as noted in the beginning of this chapter. Its steady-state speed error is much larger than the other two (see Figure 6.8 and Figure 6.13). Moreover, its transient performance is far behind the other two (Figure 6.16, Figure 6.17, Figure 6.20 and Figure 6.21). The main reason is that it proposes much stricter requirements on the current tracker and other actuators. To generate the same level torque, it requires a far larger current value than the other two which makes the system suffer from saturations of both the current tracker and the SRM more easily. However, even when there is no saturation, its steady-state and transient performance can not reach the same level attained in the other two (See Figure 6.8, Figure 6.17 and Figure 6.21). The reason behind this phenomenon is that its reference current varies much sharper than others (See Figure 6.10). Obviously, this requires that the current trackor has a very fast response ability and a quite wide bandwidth. If the current can be tracked exactly, we can conclude that there will be no other differences except the power efficiency between these methods in speed tracking. Practically, there always exists limitations for the current tracker's response capability and bandwidth. With these limitations, it is more easy for a current tracker to track a flat reference command than a sharp one. This explains why the non-optimized single-exciting has

worst performance.

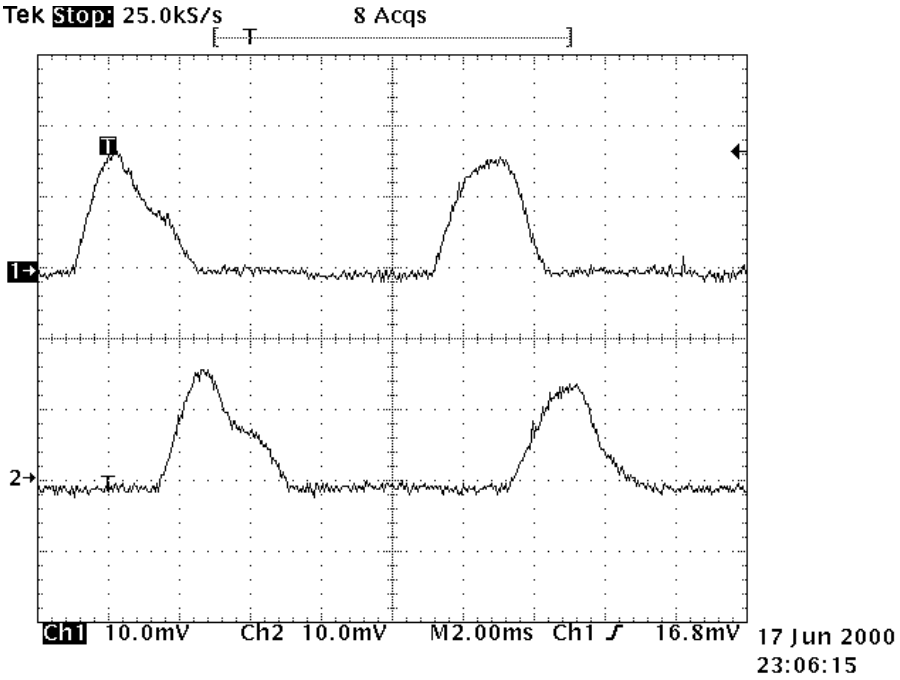

Figure 6.1: Steady-state current waveform by two-phase-exciting method at $1000RPM$. Channel 1 denotes phase A and Channel 2 is phase B with the voltage to current ratio being $1A/10mV$.

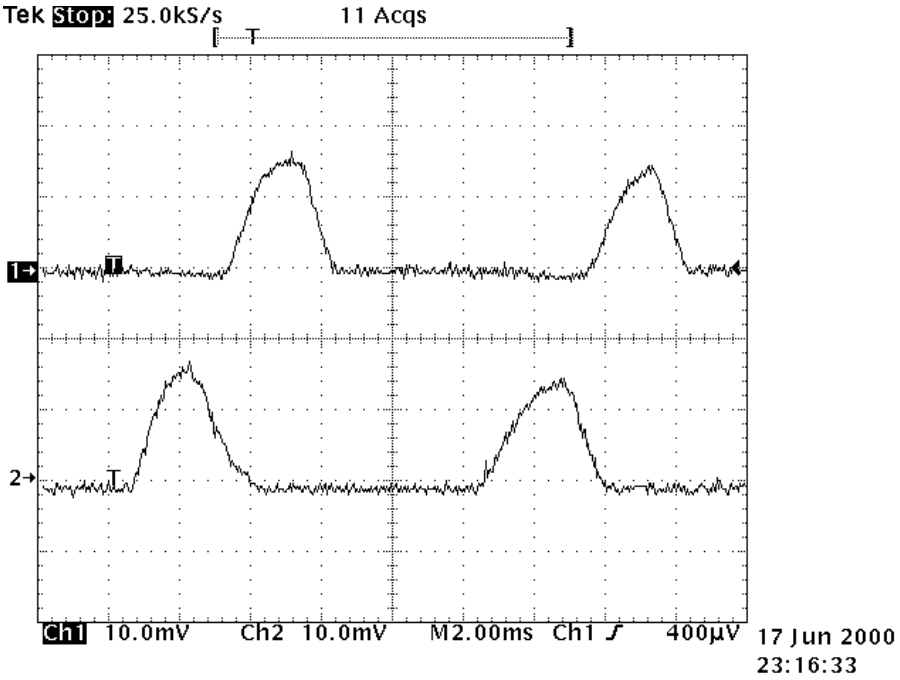

Figure 6.2: Steady-state current waveform by two-phase-exciting method at $-1000RPM$. Channel 1 denotes phase A and Channel 2 is phase B with the voltage to current ratio being $1A/10mV$.

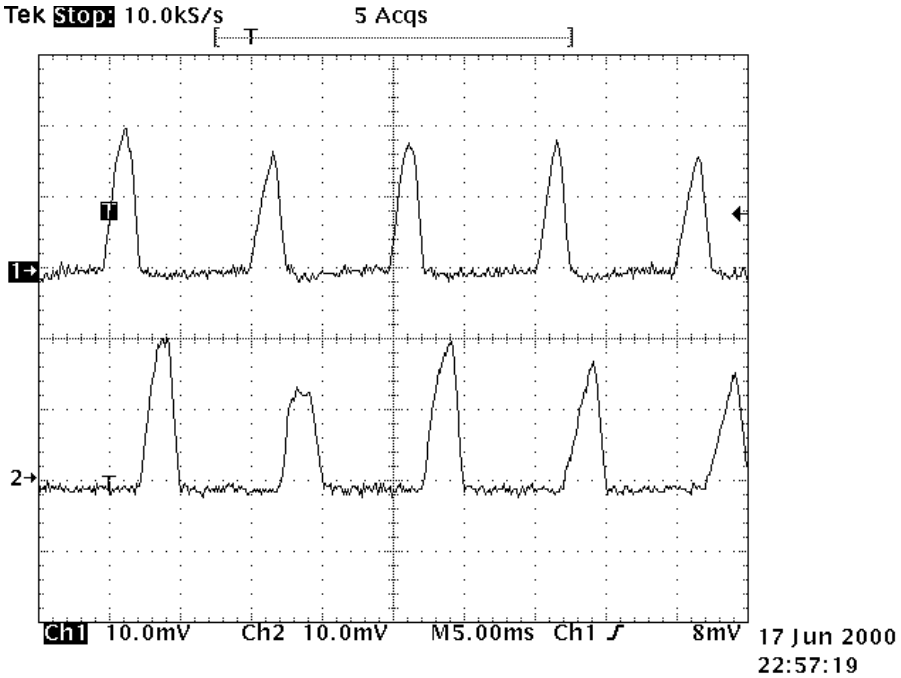

Figure 6.3: Steady-state current waveform by optimized single-phase-exciting method at $1000RPM$. Channel 1 denotes phase A and Channel 2 is phase B with the voltage to current ratio being $1A/10mV$.

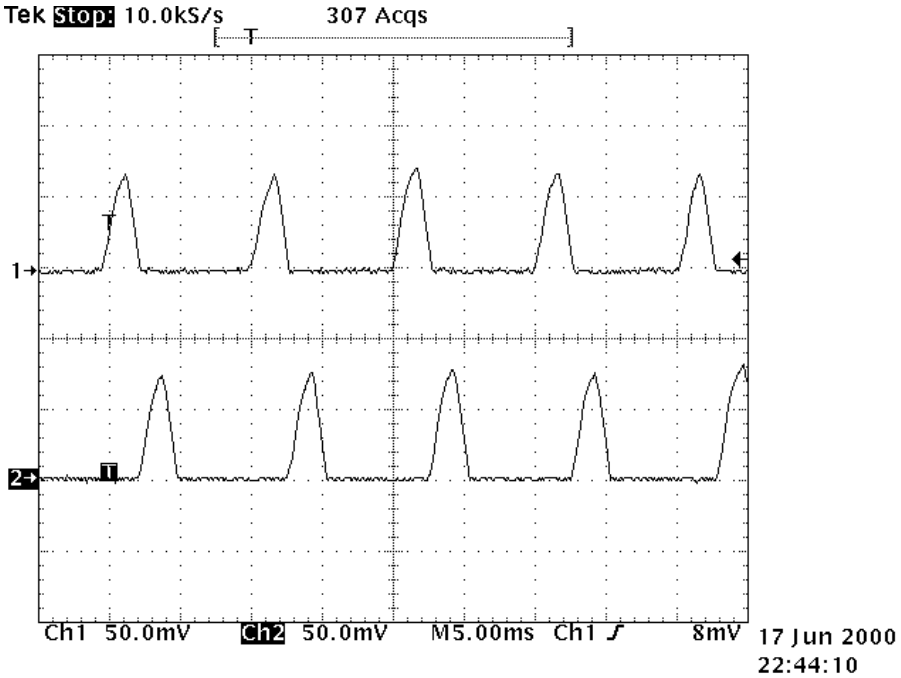

Figure 6.4: Steady-state current waveform by non-optimized single-phase-exciting method at $1000RPM$. Channel 1 denotes phase A and Channel 2 is phase B with the voltage to current ratio being $1A/10mV$.

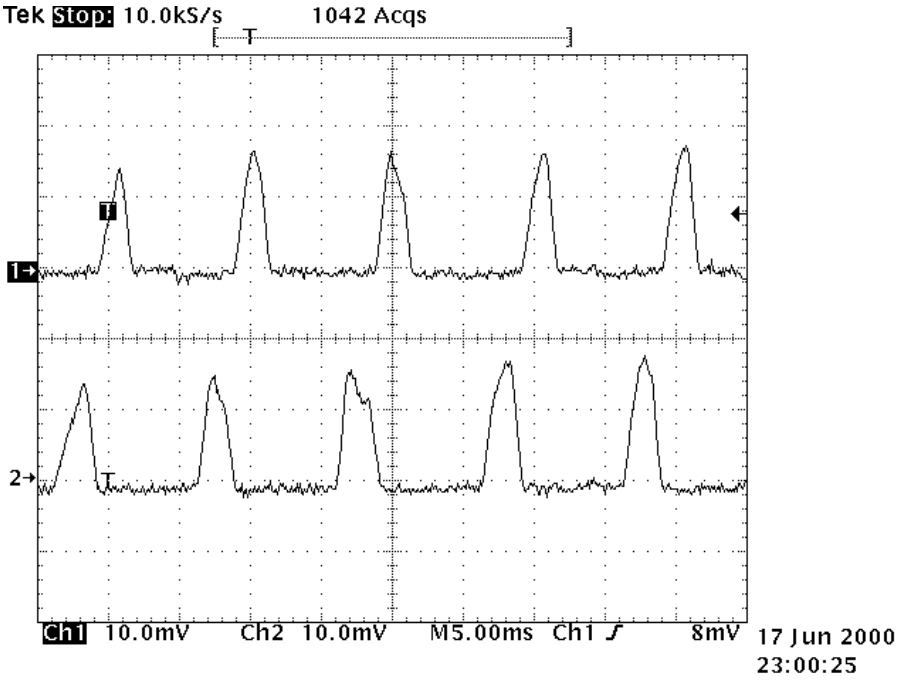

Figure 6.5: Steady-state current waveform by optimized single-phase-exciting method at $-1000RPM$. Channel 1 denotes phase A and Channel 2 is phase B with the voltage to current ratio being $1A/10mV$.

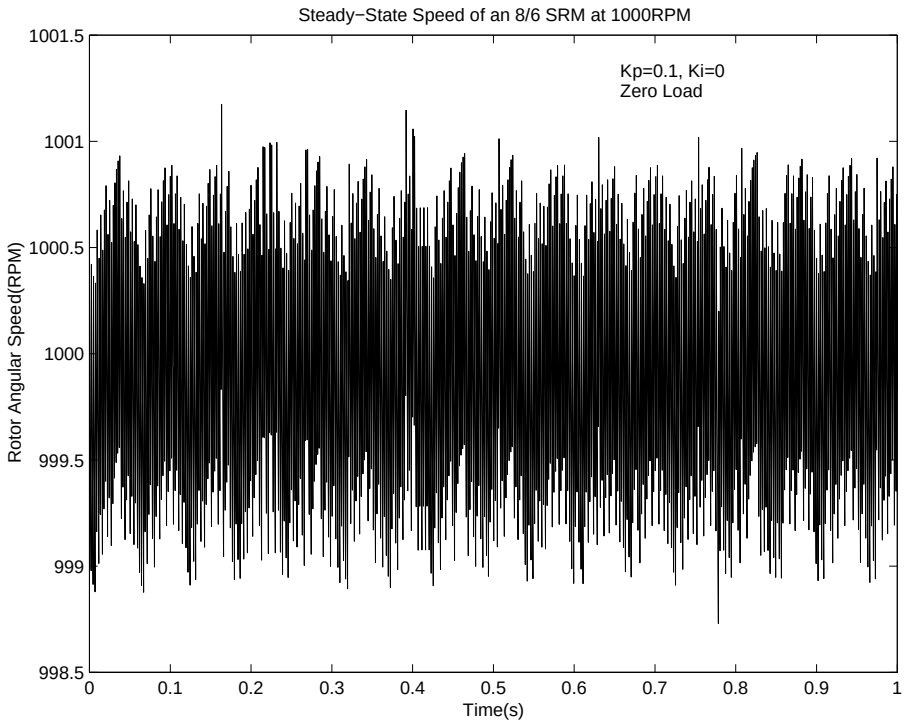

Figure 6.6: Stead-state speed waveform by two-phase-exciting method at $1000RPM$

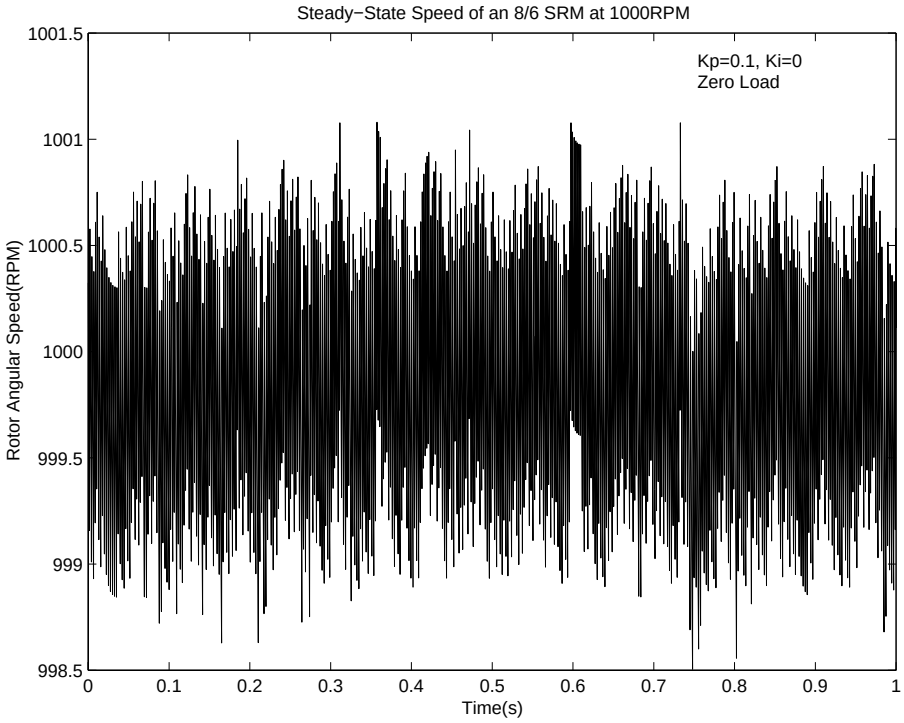

Figure 6.7: Stead-state speed waveform by optimized single-phase-exciting method at $1000RPM$

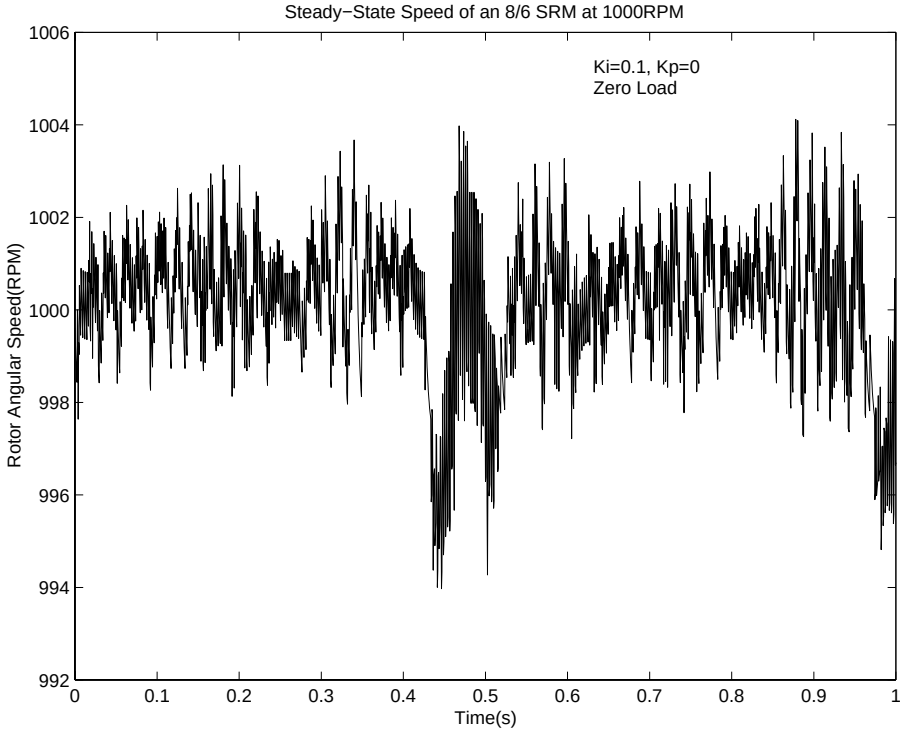

Figure 6.8: Stead-state speed waveform by non-optimized single-phase-exciting method at $1000RPM$

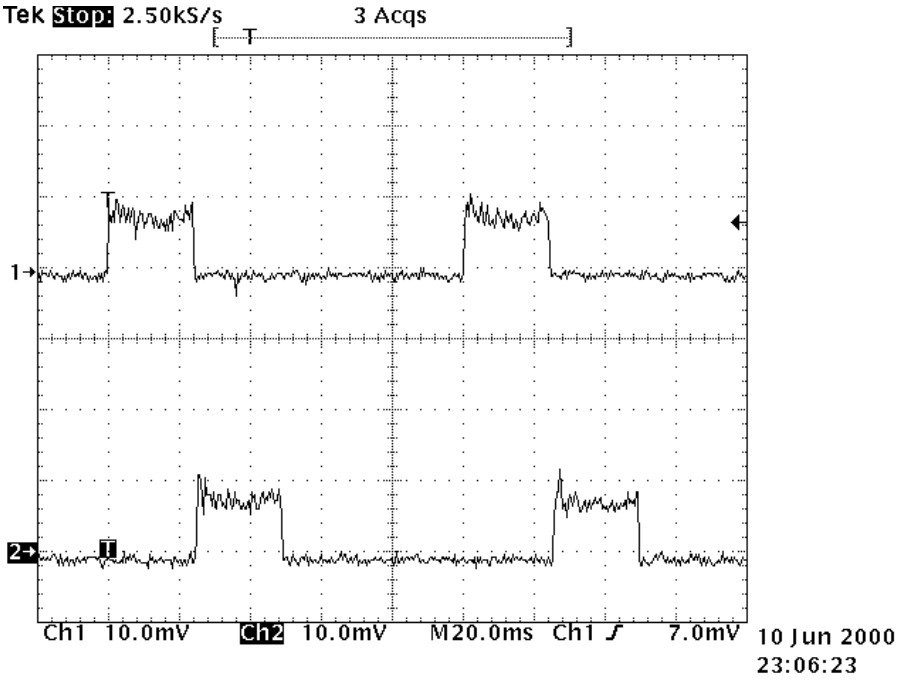

Figure 6.9: Steady-state current waveform by optimized single-phase-exciting method at $100RPM$. Channel 1 denotes phase A and Channel 2 is phase B with the voltage to current ratio being $1A/10mV$.

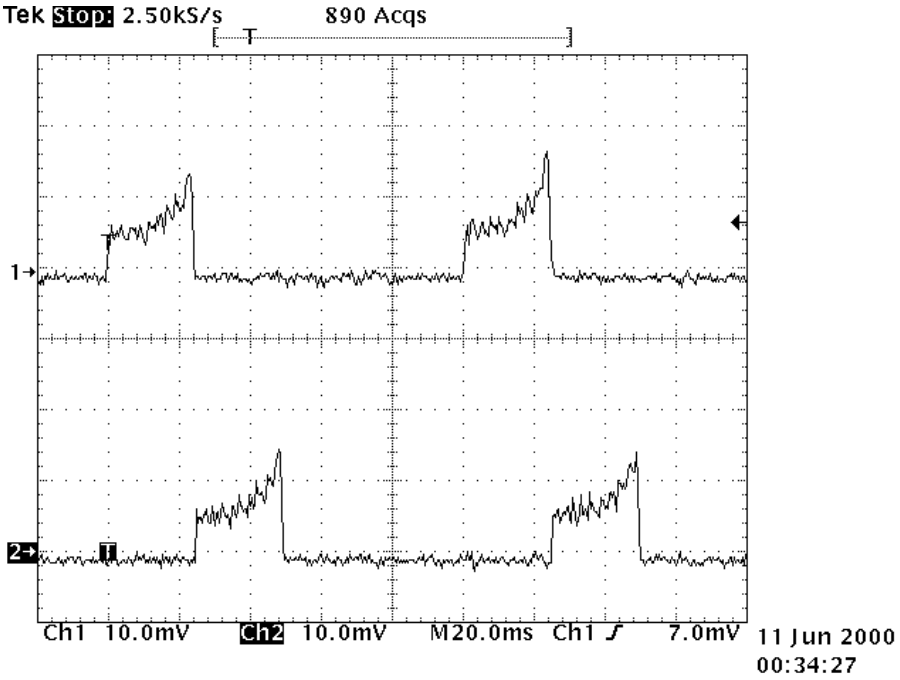

Figure 6.10: Steady-state current waveform by non-optimized single-phase-exciting method at $100RPM$. Channel 1 denotes phase A and Channel 2 is phase B with the voltage to current ratio being $1A/10mV$.

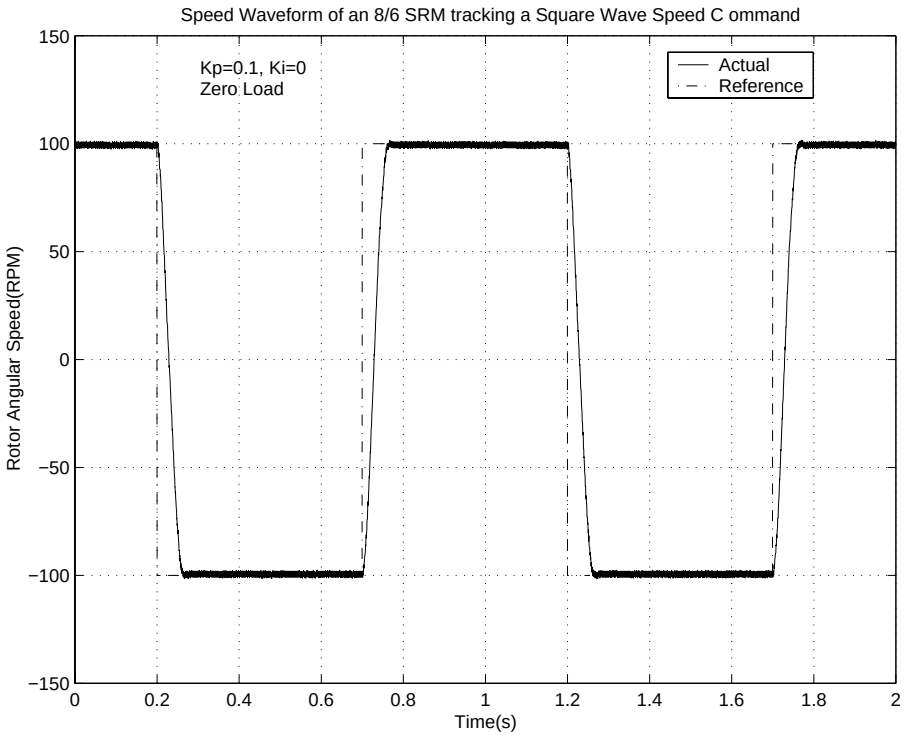

Figure 6.11: Speed waveform tracking a square wave by two-phase-exciting method at low speed

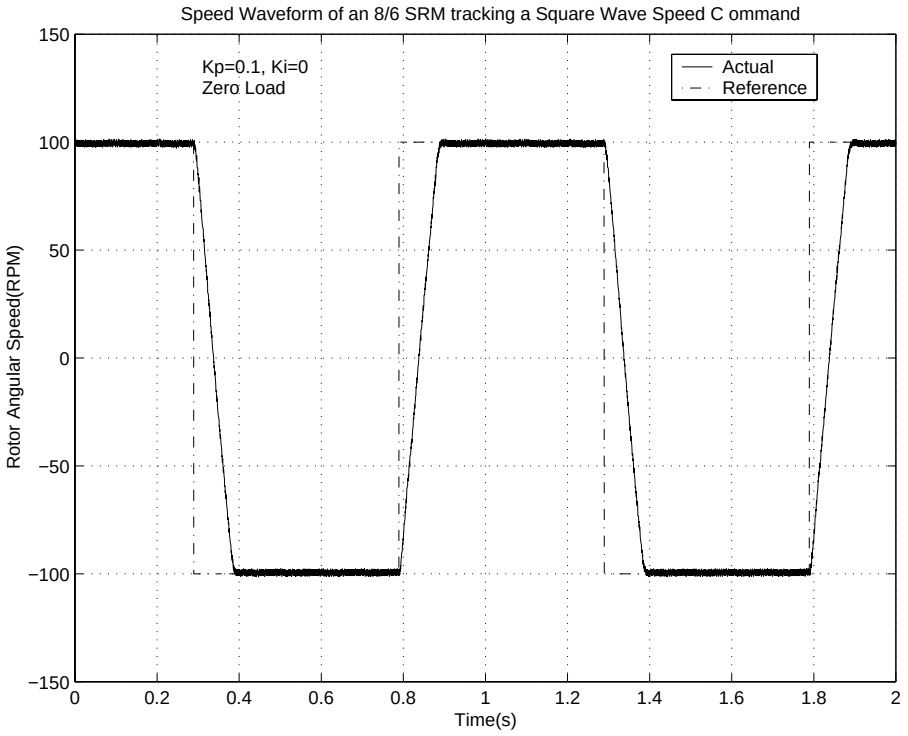

Figure 6.12: Speed waveform tracking a square wave by optimized single-phase-exciting method at low speed

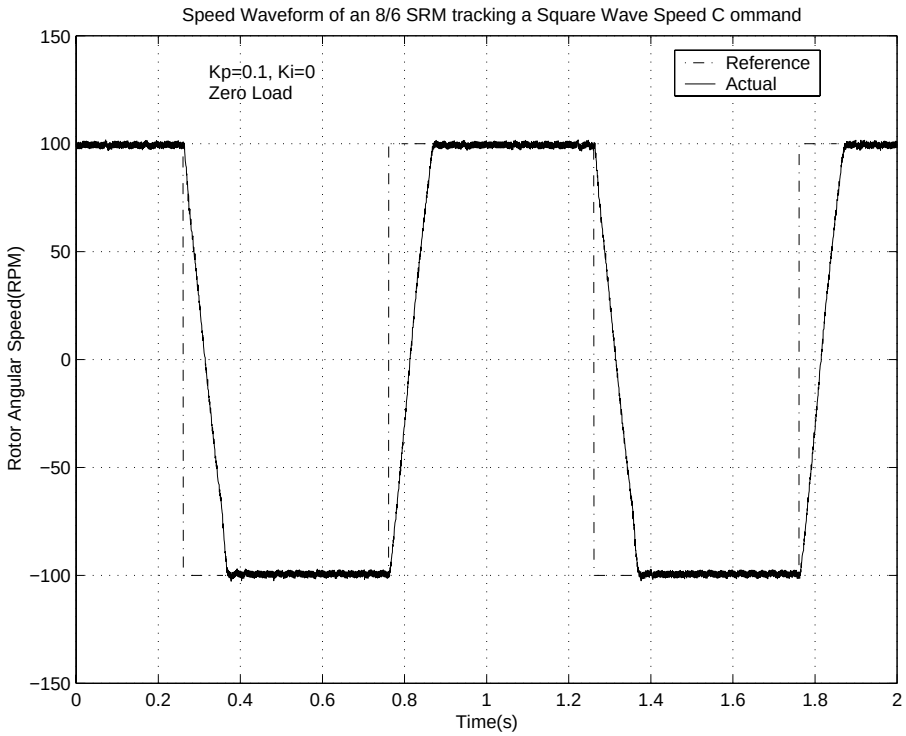

Figure 6.13: Speed waveform tracking a square wave by non-optimized single-phase-exciting method at low speed

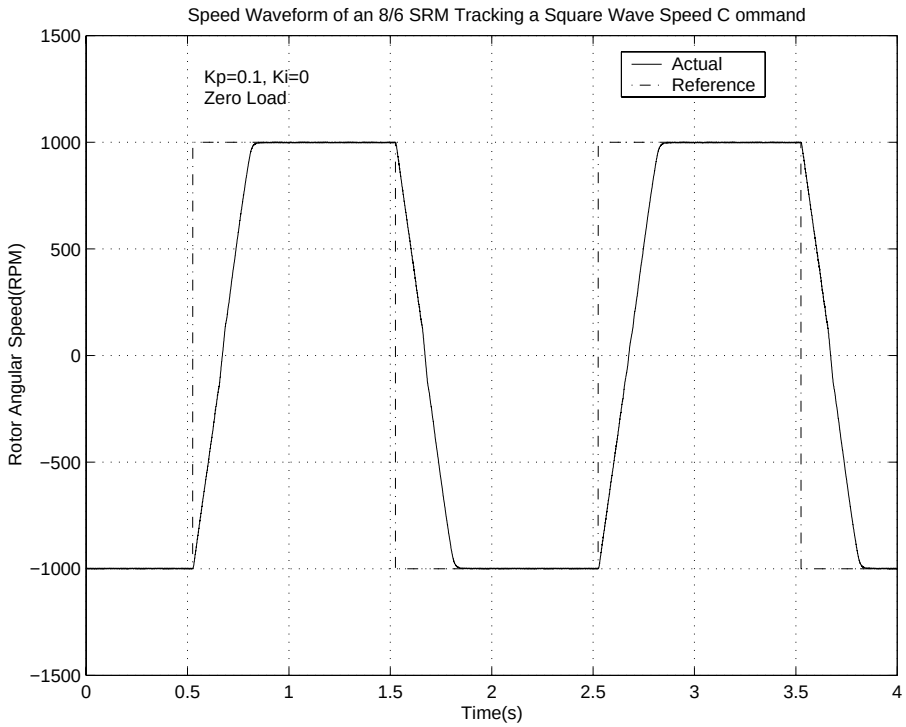

Figure 6.14: Speed waveform tracking a square wave by two-phase-exciting method

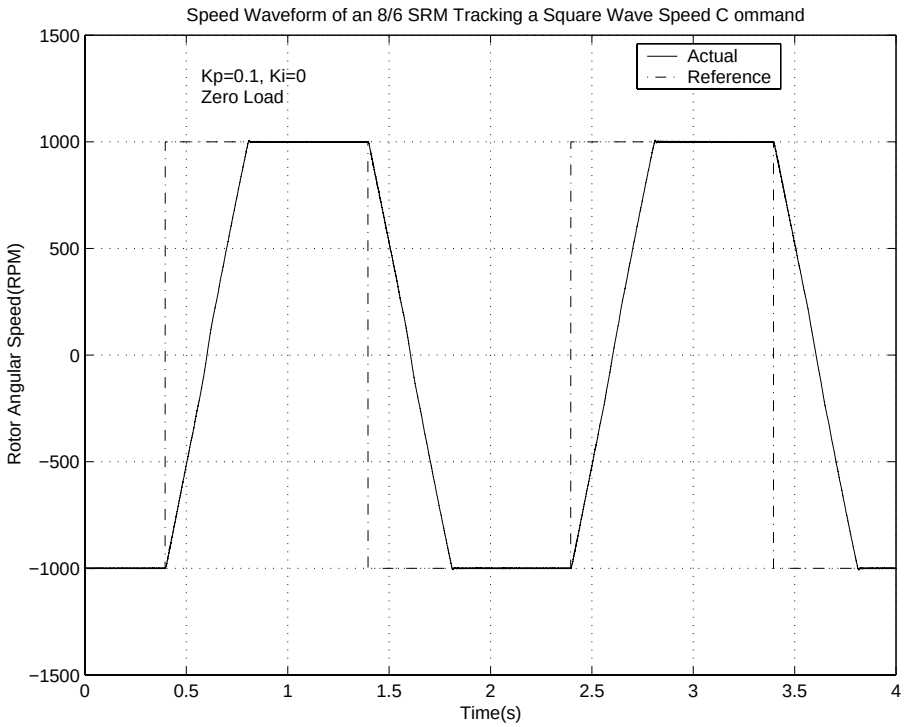

Figure 6.15: Speed waveform tracking a square wave by optimized single-phase-exciting method

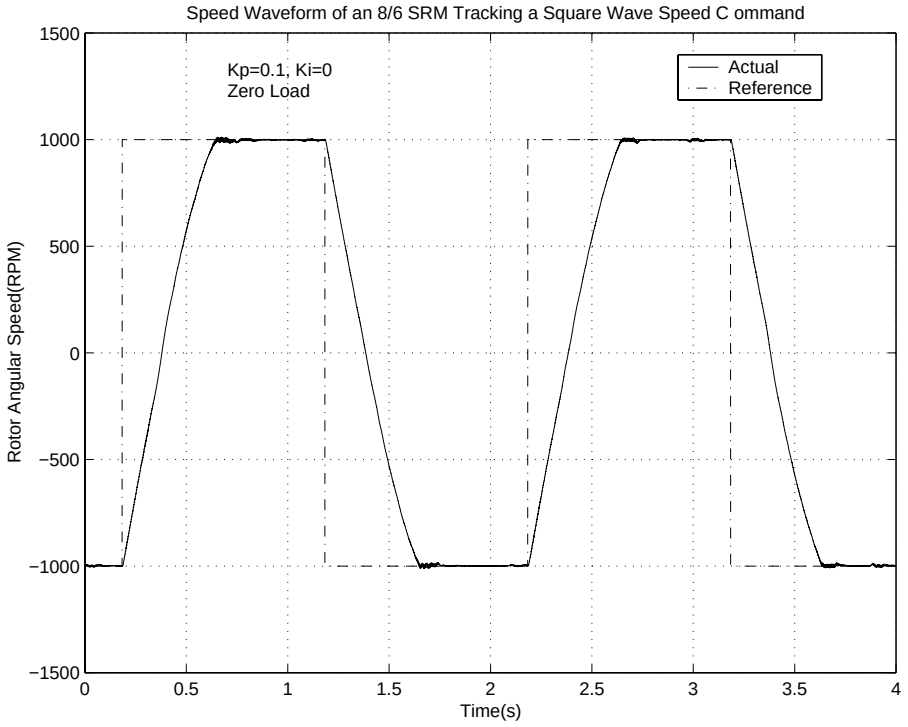

Figure 6.16: Speed waveform tracking a square wave by non-optimized single-phase-exciting method

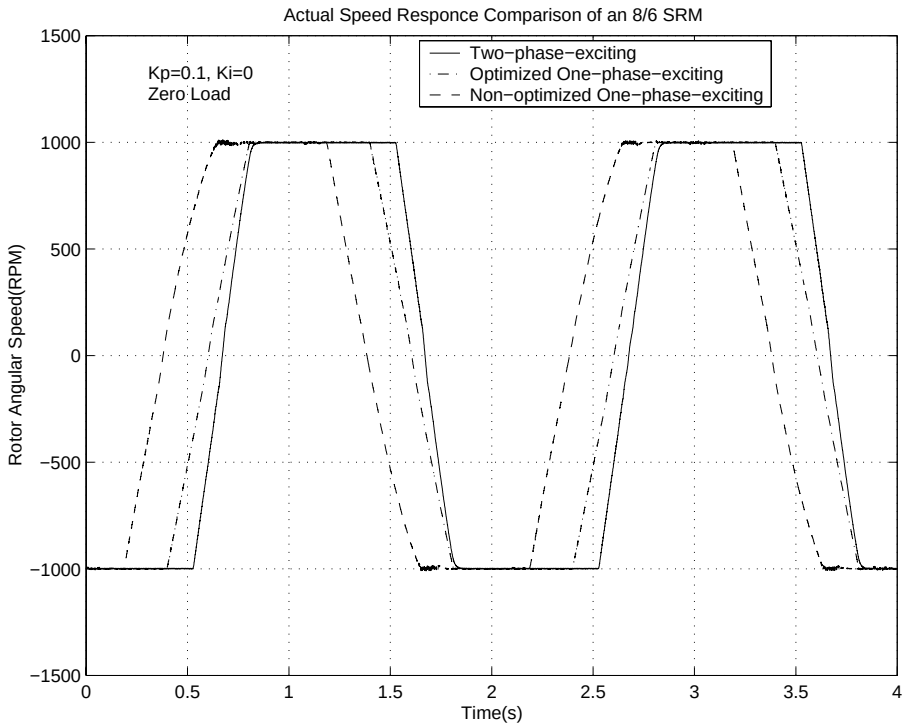

Figure 6.17: Speed Response Comparison under the same condition

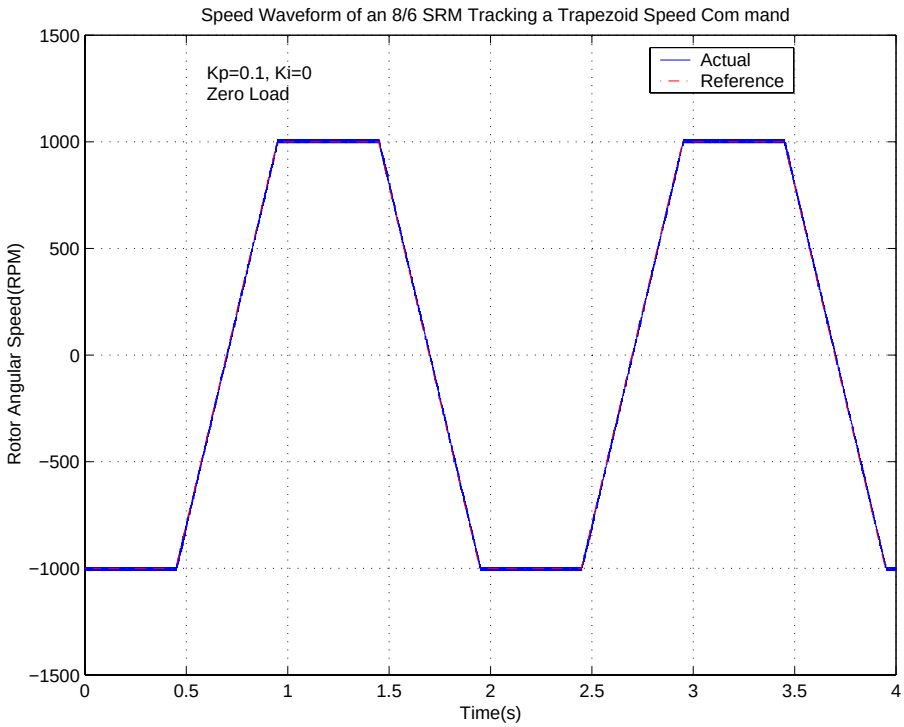

Figure 6.18: Speed waveform tracking a trapezoid wave by two-phase-exciting

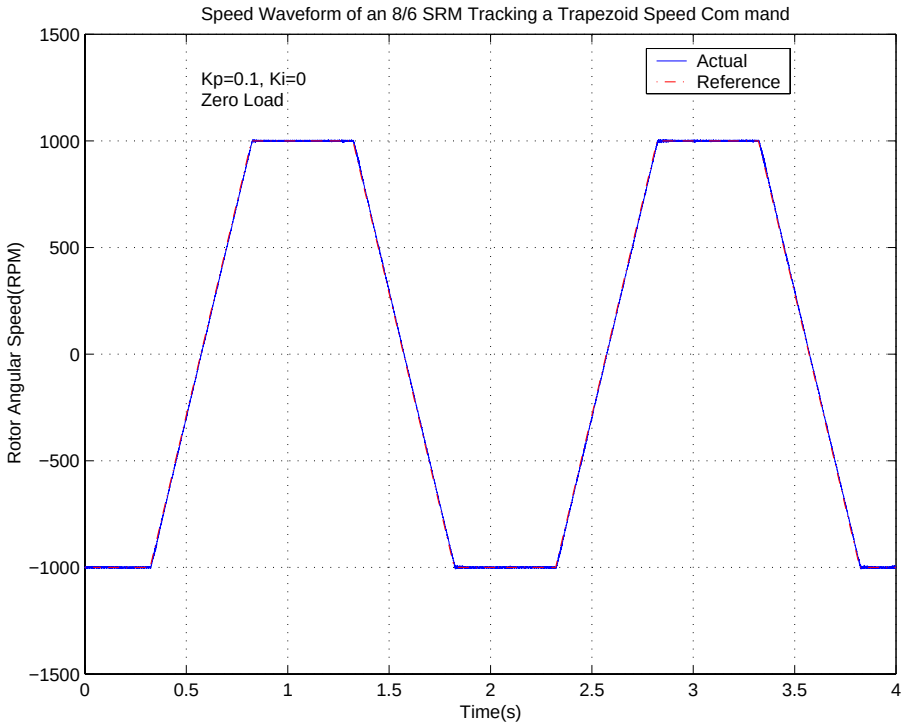

Figure 6.19: Speed waveform tracking a trapezoid wave by optimized single-phase-exciting method

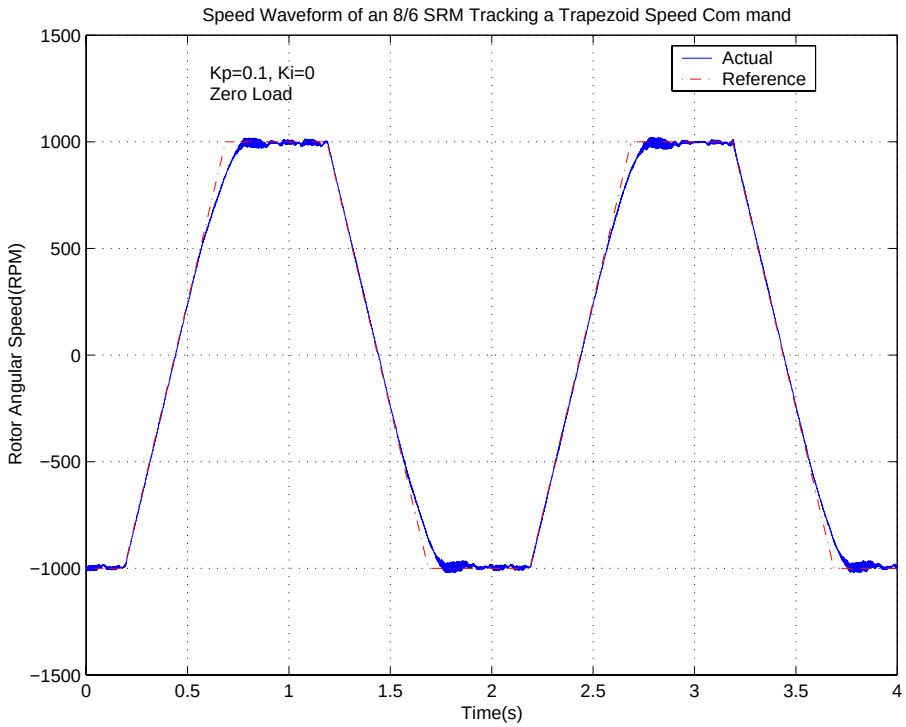

Figure 6.20: Speed waveform tracking a trapezoid wave by non-optimized single-phase-exciting

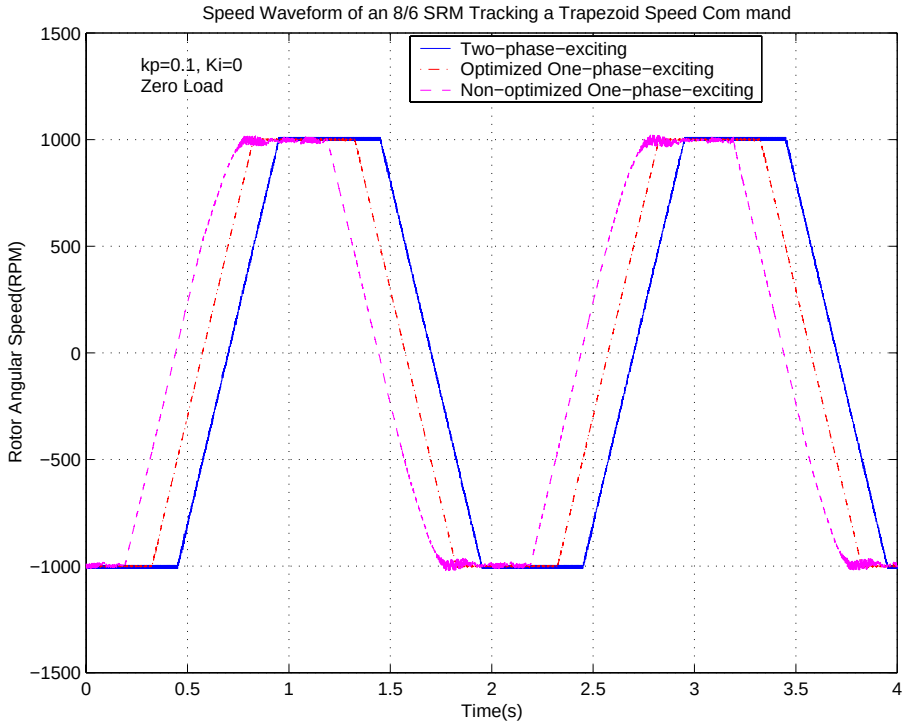

Figure 6.21: Speed waveforms comparison for tracking a trapezoid wave by different methods

Chapter 7

Conclusion and Further Work

7.1 Conclusion

This thesis gave a general introduction to switched reluctance motors control. It introduced the control of switched reluctance motors from the view of control side. Based on the general control structure (Figure 4.6), each part of this structure has been covered by thesis.

The history and structure of the SRM were introduced in the first part of this thesis. After that, it discussed the operation principles of the SRM in detail which guides the control algorithm of the SRM.

Apart from giving the general model equations of the machine, the thesis analyzed the motor's inherent special properties on the flux-linkage in Chapter 3. Also, a practical method to measure this magnetic chart has been introduced.

After the introduction, the thesis focused on the speed control of an 8/6 SRM based on a simplified model. This simplified model limits the operation of the motor totally into its linear flux region. According to this model, two different commutation strategies, two-phase exciting and single-phase-exciting methods, were compared in detail. It pointed out that, unlike the two-phase-exciting, the turn-on angle for single-phase-exciting is not trivial as it will affect the system performance. Consequently, an optimized single-phase-exciting

method was proposed. This method can optimize the power efficiency of the whole system.

Following the description of experimental hardware set up, experimental results were demonstrated to support the proposed method. These results compared the influences of the two-phase-exciting strategy, optimized and non-optimized single-phase-exciting method on the speed tracking capacity and stator currents. It showed that the optimized single-phase has almost the same speed tracking capacity as the two-phase-exciting strategy, and the peak value of their stator currents is at the same level under the same condition. However, the speed tracking ability of the non-optimized single-phase-exciting method is not as strong as that of the other two. It turned out that the stator currents by this method is much larger than the others, which proposes stricter requirements on the current tracker. What is more, it is apt to suffer from saturation effect both of the SRM and actuators. This is the reason why its transient and steady-state performance is worse than the other two.

7.2 Further Work

As discussed before, the control of the switched reluctance motor is a very big topic which contains a lot of challenging issues. From the view of this thesis, further research can be performed as the following:

1. In this thesis, we compared how the one-phase-exciting and two-phase-exciting methods affect the motor's performance such as the stator current per phase and dynamical response. However, which method can help torque ripple reduction is left undiscussed. It is not difficult to conclude that the two-phase-exciting algorithm can help reduce toque ripple because the current during the commutation period in two-phase-exciting can be well controlled, however, how and to what extent these methods affect the torque ripple has to be investigated for high performance motor control.

2. New methods to improve the motor's dynamical performance should be investigated. The experimental results show that the PI controller is not enough for high speed, heavy load cases since it can't optimize the transient current, which will cause actuator saturation and become the critical limitation of improving the SRM' dynamical performance. Hence, new controllers should be developed. Two degree of freedom controller, robust controller, artificial- neutral-network controller, fuzzy controller and so on may be possible solutions.

3. The control algorithm of this project is completely based on the model in the linear flux-linkage region. It ignored the motor's saturation effect. However, the experimental results show that we can't guarantee the SRM being operated completely in this linear region. Actually, to meet fast dynamics requirements, the stator currents usually are large enough to go beyond the linear flux region. However, the model used in this thesis did not and could not take this fact into account. Undoubtedly, this saturation effect affects the motor's transient performance. Hence, the transient is not as good as expected. Therefore, advanced modeling method should be developed to take care the saturation effect to achieve better performance.

4. In this thesis, the commutation of the SRM is based on precise position sensoring device, position encoder. As mentioned before, the motor's flux-linkage is a function of stator currents as well as rotor position. For fixed stator current, the relationship between the flux-linkage and rotor position is also fixed for the same motor. So once obtaining the flux chart as discussed in chapter 3, the rotor position can be estimated by measuring the stator currents and voltages. Hence, position sensorless algorithm can be investigated.

Chapter 8

Photo Album

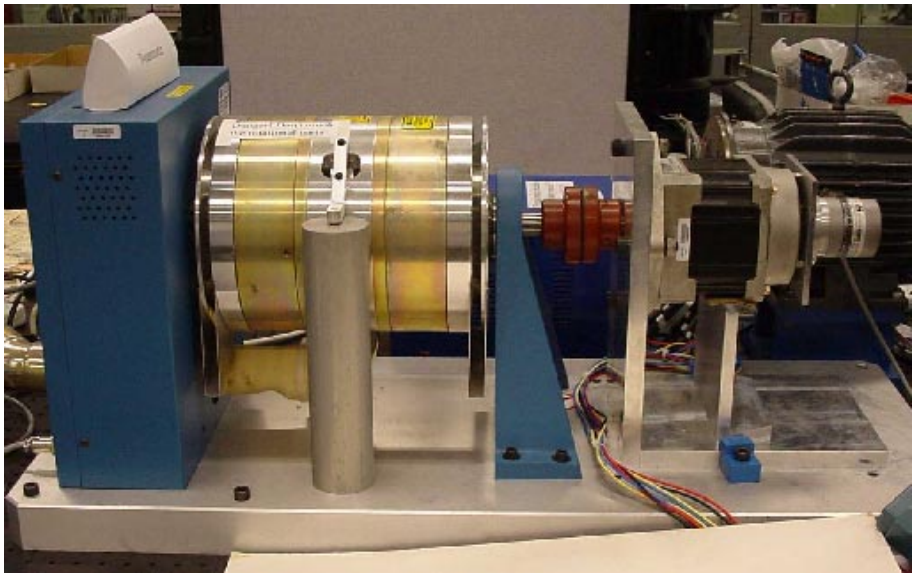

Figure 8.1: The Switched Reluctance Motor and Dynameter

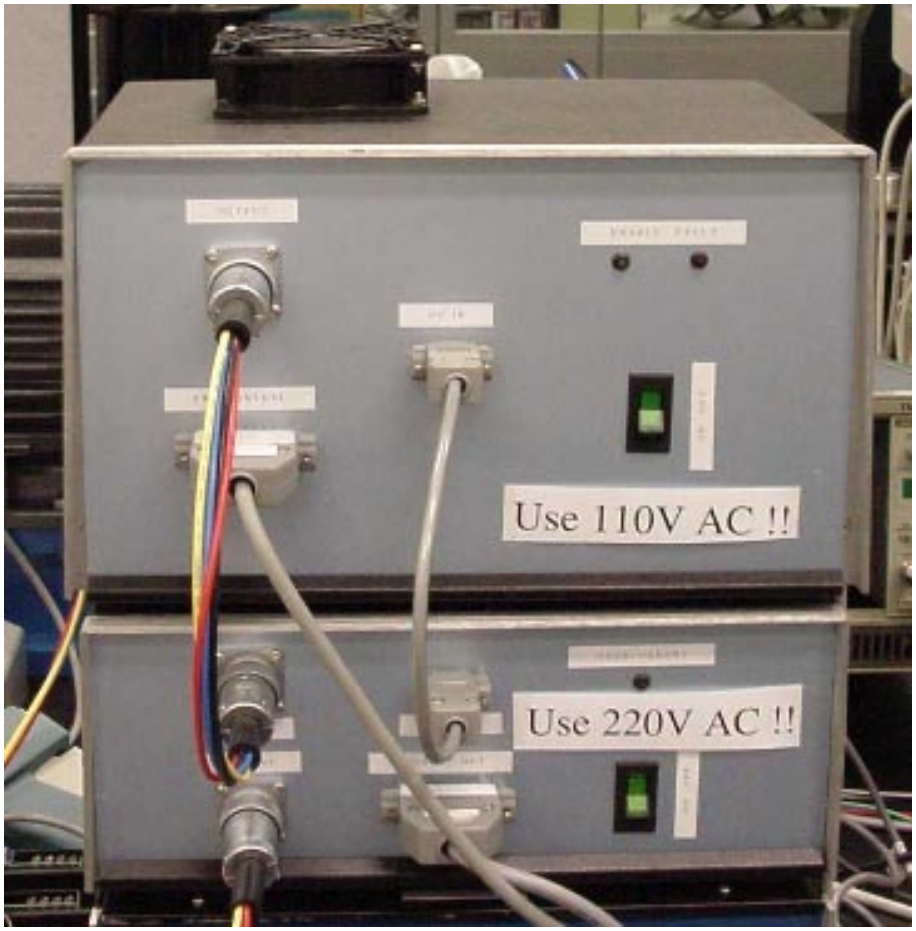

Figure 8.2: The Current Driver and Sensor Devices

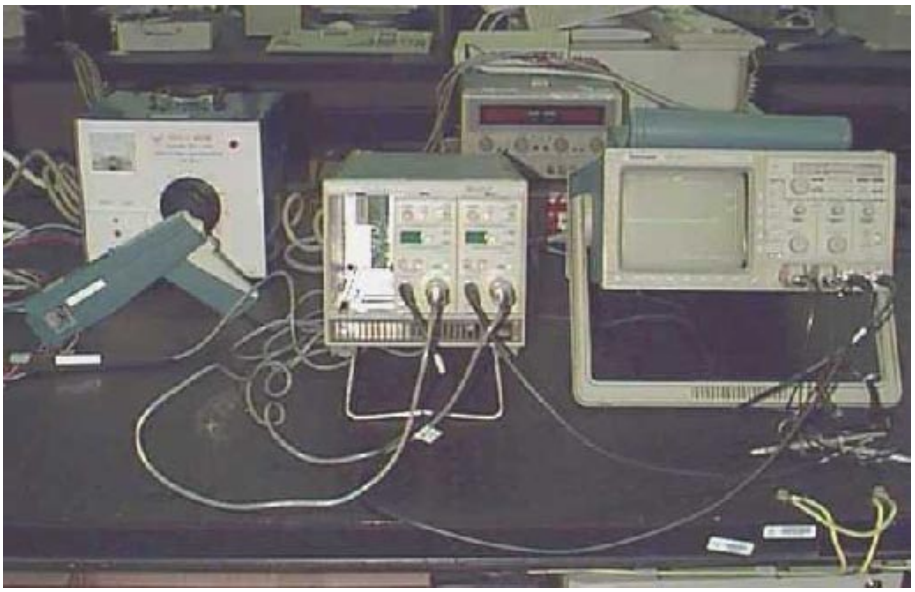

Figure 8.3: Current Sensoring Devise for Monitor: Current Probe

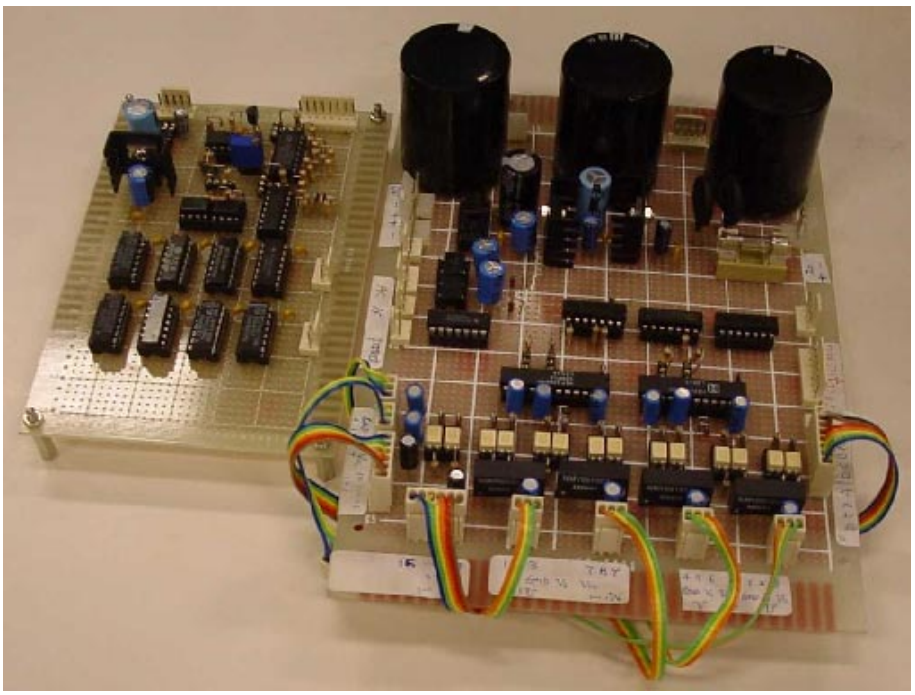

Figure 8.4: The Switched Reluctance Motor's Driving Board

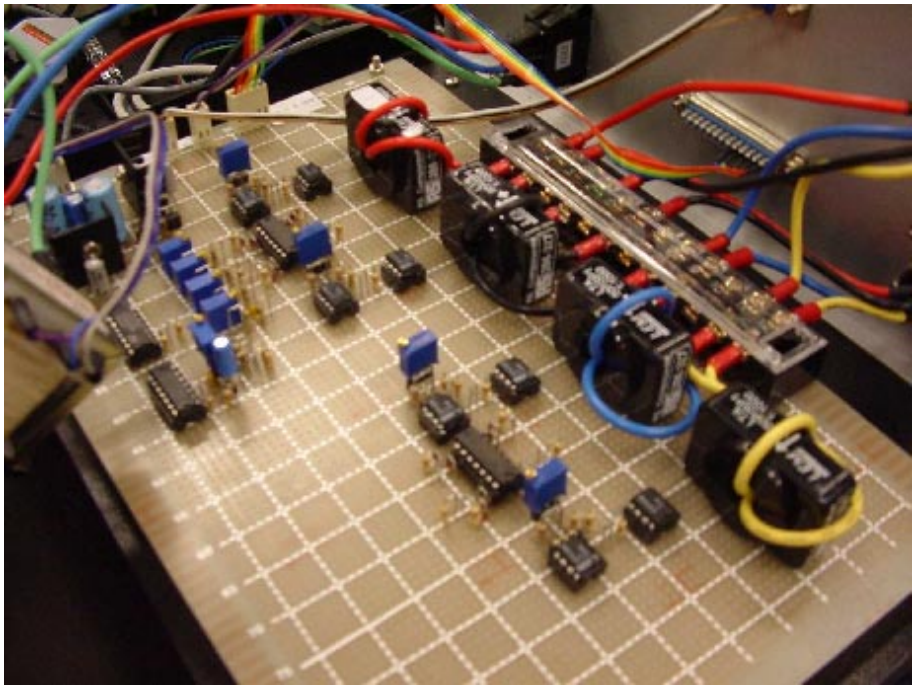

Figure 8.5: Current Sensoring Board

Bibliography

[1] S.A. Nasar, "DC Switched Reluctance Motor", *Proceedings of the Institution of Electrical Engineers*, vol.166, no.6, June, 1996, pp.1048-1049.

[2] J.V. Byrne, et al., "A High Performance Variable Reluctance Drive: A New Brushless Servo", *Motor Control Proceedings*, Oct. 1985, pp.147-160.

[3] P.French and A.H. Williams, "A New Electric Propulsion Motor", *Proceedings of AIAA Third Propulsion Joint Specialist Conference*, Washington, D.C., July, 1967.

[4] L.E. Unnewehr and H.W. Koch, "An Axial Air-Gap Reluctance motor for Variable Speed Application", *IEEE Transactions on Power Apparatus and Systems*, vol.PAS-93, no.1, January, 1974, pp.367-376.

[5] P.J. Lawrenson, "Switched Reluctance Motor Drives", *Electronics and Power*, 1983, pp.144-147.

[6] T.H. Liu, Y.J. Chen and M.T. Lin, "Vector Control and Reliability Improvement for a Switched Reluctance Motor", *Proceedings of the IEEE International Conference on Industrial Technology*, 1994, pp.538-542.

[7] T.H. Liu, Y.J. Chen and M.T. Lin, "A High Performance Field-Oriented Control for a Switched Reluctance Motor Drive", *Proceedings of 1995 International Conference on Power Electronics and Drive Systems*, 1995, vol.1, pp.180-185.

[8] N. Matsui, N. Akao and T. Wakino, "High-Precise Torque Control of Reluctance Motors", *IEEE Transactions on Industry Applications*, vol.27, no.5, Sep/Oct., 1991.

[9] T.J.E. Miller, *Switched Reluctance Motors and Their Control*, Magna Physics and Clarendon Press, Oxford, 1993.

[10] S.A. Nasar, I. Boldea and L.E. Unnewehr, *Permanent Magnet, Reluctance, and Self-synchronous Motors*, Boca Raton, Fla., CRC Press, 1993.

[11] V. Ramanarayanan, L. Venkatesha and D. Panda, "Flux Linkage Characteristics of Switched Reluctanct Motors", *Proceedings of IEEE Conference PEDES'96*, New Delhi, India, Jan., 1996, pp.281-285.

[12] V.K. Sharma, S.S. Murthy and B. Singh, "An Improved Method for the Determination of Saturaion Characteristics of Switched Reluctance Motors", *IEEE Transactions on Instrum. and Meas.*, vol. 48, no. 5, Oct., 1999, pp.995-1000.

[13] L.Y. Xu and J.R. Bu, "Position Transducerless Control of a Switched Reluctance Motor Using Minimum Magnetizing Input", *IAS '97. Conference Record of the 1997 IEEE Industry Applications Conference Thirty-Second IAS Annual Meeting, IEEE*, Part vol.1, 1997, pp.533-539, vol.1. New York, NY, USA.

[14] P.J. Zhan, C.C. Chan and K.T. Chau, "A Novel Sliding-Mode Observer for Indirect Position Sensing of Switched Reluctance Motor Drives", *IEEE Transactions on Industrial Electronics*, vol.46, no.2, April 1999, pp.390-397.

[15] Kosaka, K. Ochiai and N. Matsui, "Sensorless Control of SRM Using Magnetizing Curves", *Transactions of the Institute of Electrical Engineers*, Japan, Part D, vol.120-D, no.2, Feb. 2000, pp.216-222.

[16] I.W. Yang, J.W. Shin and Y.S. Kim, "The Rotor Speed and Position Sensorless Control of Switched Reluctance Motor Using the Adaptive Observer", *Proceedings of IEEE. IEEE Region 10 Conference TENCON 99. 'Multimedia Technology for Asia-Pacific Information Infrastructure' IEEE.* Part vol.2, 1999, pp.1450-1453 vol.2. Piscataway, NJ, USA.

[17] G. Suresh, B. Fahimi, K.M. Rahman, M. Ehsani and I. Panahi, "Four-quadrant Sensorless SRM Drive With High Accuracy at All Speeds", *APEC '99. Fourteenth Annual Applied Power Electronics Conference and Exposition. 1999 Conference Proceedings IEEE.* Part vol.2, 1999, pp.1226-1231, Piscataway, NJ, USA.

[18] N.J. Nagel and R.D. Lorenz, "Rotating Vector Methods for Sensorless, Smooth Torque Control of a Switched Reluctance motor Drive", *Conference Record of 1998 IEEE Industry Applications Conference. Thirty-Third IAS Annual Meeting, IEEE.* vol.1, 1998, pp.723-730, New York, NY, USA.

[19] D.G. Taylor, "Adaptive Control Design for a Class of Doubly-Salient Motors", *Proceeding of the 30th Conference on Decision and Control,IEEE.* , 1991, vol.3, pp.2903-2908.

[20] D. M. Dawson, J. Hu and T.C. Burg, *Nonlinear Control of Electric Machinery*, Marcel Dekker Inc., 1998, pp.105-137.

[21] L. Y. Xu and J.R. Bu, "Analysis of a Novel Converter Topology for Switched Reluctance Machine Drives", *Proceedings of the IEEE International Conference on Power Electronics, Drives & Energy Systems for Industrial Growth, Pedes.* vol. 2, 1998, pp.640-645.

[22] W. Leonhard, *Control of Electrical Drives*, Springer-Verlag, 2nd edition, 1996.

[23] H. K. Bae and R. Krishnan, "A Study of Current Controllers and Development of a Novel Current Controller for High Performance SRM Drives",

IAS'96. Conference Record of the 1996 IEEE Industry Applications Conference, Thirty-First IAS Annual Meeting, IEEE, vol.1, 1996, pp.68-75, New York, NY, USA.

[24] *Proceedings of Symposium on Industrial Drives and Traction*. IEEE PES/IAS Jiont Chapter (HK Section), November, 1996.

[25] C.C. Chan and Q. Jiang, "Study of Starting Performances of Switched Reluctance Motors", *IEEE Proceedings of 1995 International Conference on Power Electronics and Drive Systems*, 1995, vol.1, pp.174-179.